Published in final edited form as:
Biomacromolecules. 2012 November 12; 13(11): 3627–3640. doi:10.1021/bm301583s.

Dextran Vesicular Carriers for Dual Encapsulation of Hydrophilic and Hydrophobic Molecules and Delivery into Cells

P. S. Pramod[†], **Kathryn Takamura**[‡,§], **Sonali Chaphekar**[‡], **Nagaraj Balasubramanian**[*,‡], and **M. Jayakannan**[*,†]

[†]Department of Chemistry, Indian Institute of Science Education and Research (IISER), Pune Dr. Homi Bhabha Road, Pune–411008, Maharashtra, India

[‡]Department of Biology, Indian Institute of Science Education and Research (IISER), Pune Dr. Homi Bhabha Road, Pune–411008, Maharashtra, India

Abstract

Dextran vesicular nanoscaffolds were developed based on polysaccharide and renewable resource alkyl tail for dual encapsulation of hydrophilic and hydrophobic molecules (or drugs) and delivery into cells. The roles of the hydrophobic segments on the molecular self-organization of dextran backbone into vesicles or nanoparticles were investigated in detail. Dextran vesicles were found to be a unique dual carrier in which water-soluble molecules (like Rhodamine-B, Rh-B) and polyaromatic anticancer drug (camptothecin, CPT) were selectively encapsulated in the hydrophilic core and hydrophobic layer, respectively. The dextran vesicles were capable of protecting the plasma-sensitive CPT lactone pharmacophore against the hydrolysis by 10× better than the CPT alone in PBS. The aliphatic ester linkage connecting the hydrophobic tail with dextran was found to be cleaved by esterase under physiological conditions for fast releasing of CPT or Rh-B. Cytotoxicity of the dextran vesicle and its drug conjugate were tested on mouse embryonic fibroblast cells (MEFs) using MTT assay. The dextran vesicular scaffold was found to be nontoxic to living cells. CPT loaded vesicles were found to be 2.5-fold more effective in killing fibroblasts compared to that of CPT alone in PBS. Confocal microscopic images confirmed that both Rh-B and CPT loaded vesicles to be taken up by fibroblasts compared to CPT alone, showing a distinctly perinuclear localization in cells. The custom designed dextran vesicular provides new research opportunities for dual loading and delivering of hydrophilic and hydrophobic drug molecules.

Introduction

Polymer-based drug delivery approaches are emerging as an important methodology for the administration of medicines or genes for cancer diseases.1,2 The leaky and uncontrolled growths of the cancer tissues facilitate the preferential accumulation of polymer–drug

[*]**Corresponding Author**: nagaraj@iiserpune.ac.in (N.B.); jayakannan@iiserpune.ac.in (M.J.). Fax: +91-20-2590 8186 (M.J.).
[§]**Present Address**
Research Student, Department of Biochemistry, The Ohio State University, 776 Biological Sciences Building, 484 West 12th Avenue, Columbus, Ohio 43210, United States.

The authors declare no competing financial interest.

Europe PMC Funders Author Manuscripts

conjugate via enhanced permeability and retention (EPR) effect.3 Amphiphilic polymers or block copolymers were employed for this purpose typically self-organize into nanoscaffolds such as micelles, hydrogels, and vesicles (or polymersomes) in which polyaromatic drug molecules are encapsulated and later delivered into the specific site or organ.4 Among the various self-organized forms, especially polymer vesicles provide several technological advantages such as efficient cell penetrating ability, longer blood circulation time, resistance against plasma proteins, and so on.5 Further, the synthetic vesicles resemble the structure of the biological cell membranes, which enhanced their cellular uptake through like-interactions.6 The synthesis of amphiphilic polymers were typically achieved by anchoring hydrophobic moieties on the water-soluble polysaccharides or polyethylene glycol backbones.7 According to the empirical rule proposed by Eisenberg; amphiphilic copolymers having more than 45% hydrophilic contents produced spherical micelles whereas vesicles or inverted nanostructures were formed for 35 or <25% of hydrophilic contents, respectively.8 Recent studies revealed that it was rather difficult to apply general principles to predict the molecular self-organization in polysaccharides.9 This was partially associated with the uncontrolled secondary interactions lead by the hydroxyl groups in the polymer backbone, which leads to the premature collapsing of vesicular structures.9 Polysaccharides like dextran have been extensively employed in clinics for more than five decades as antithrombolytic agents, MRI contrast components, plasma volume expanders, and so on.10 Therefore, suitable modification of this clinically useful polysaccharide-dextran into amphiphilic copolymers and self-organizing them as nanoscaffolds for drug delivery is much in demand.11 Earlier, a few efforts had been taken to functionalize dextran with alkyl chains or long polymers through ester or acetal linkages12 for biomedical application such as hydrogels.13 Most of these modified dextrans were found to be self-organized as nanoparticles or micelles; as a result, polysaccharide vesicles were less explored for drug delivery.14 Recently, Schatz et al. reported polysaccharide–peptide block copolymer vesicles as viral capsids.15 In general, approaches to make dextran vesicles are not explored much in the literature; as a result, polysaccharide-based vesicles (or polymersomes) are one of the least explored polymer vectors for drug delivery.

The present investigation is emphasized to develop “dual encapsulating dextran vesicles” as carrier for drug loading and delivering hydrophilic as well as hydrophobic molecules (or drugs) into cells. The present design strategy is also unique and is one of the first examples of this kind in which both the hydrophilic polymer backbone and hydrophobic tails were chosen from naturally available resources (see Figure 1). Cashew nut shell liquid (CSNL) is a renewable resource industrial waste enriched with long aliphatic C_{15} chains containing phenols. Earlier, various research groups, including ours, had explored CNSL as intermediates for the synthesis of polymers, nanomaterials, gels, and so on.16 However, no attempt has been made for their application in drug delivery research. Herein, 3-pentadecylphenol (PDP) and its unsaturated counterpart cardanol, two main components of CNSL were anchored via aliphatic ester linkage to the dextran backbone through tailor-made synthetic approaches. Additionally, commercially available stearic acid (SA) was also utilized to derivatize dextran; so that the role of hydrophobic anchoring unit on the molecular self-organization of dextran into vesicles or nanoparticles could be established. It was found that those amphiphilic dextran derivatives were self-organized in water to form

~120 nm vesicles. Further, single crystal structure was resolved to establish the role of PDP-chain hydrophobic tail interactions in the formation of unilamellar vesicular structures. The dextran vesicular scaffolds were capable of loading hydrophilic molecules (Rhodamine-B, Rh-B, water-soluble dye) and hydrophobic polyaromatic anticancer drug (Camptothecin, CPT; see Figure 1). The stability of the CPT enhanced in the vesicular structure almost 10-fold compared to its isolated form. Esterase when used as stimuli to break the polymer scaffold was seen to release CPT or Rh-B from the vesicular scaffolds at significantly much faster rate. Cellular uptake of both Rh-B and CPT loaded vesicular scaffolds were investigated in mouse embryonic fibroblasts (MEFs). Both were found to be efficiently taken up by cells with CPT drug and were found to be 2.5-fold more efficient in killing the cells when loaded in the vesicular scaffold compared to CPT alone. Confocal microscope images gave further evidence for the cellular uptake of dextran vesicles and their selective perinuclear localization in cells. The present approach opens up new drug delivery concept based on polysaccharide vesicles, more specifically in dextran vesicles, for stabilizing and delivering both hydrophobic drugs and hydrophilic molecules inside the cells.

Experimental Section

Materials

Dextran (M_w = 6000), 3-pentadecylphenol, stearic acid, dicyclohexylcarbodiimide, 4-dimethylamino pyridine, pyrene, 20-(*S*)-camptothecin (CPT), and horse liver esterase enzyme were purchased from Aldrich chemicals. Cardanol was purchased locally and purified by double distillation, followed by column chromatograpy. Dimethyl sulphoxide was dried over CaH_2 and distilled prior to use. Ethyl chloroacetate, K_2CO_3, KI, KOH, and all other reagents and solvents were purchased locally and purified following the standard procedure. Wild-type mouse embryonic fibroblasts were maintained in DMEM (phenol red free medium: Gibco) containing 10% (v/v) fetal bovine serum (FBS) and 1% (v/v) penicillin–streptomycin at 37 °C under a 5% CO_2 humidified atmosphere. Cells were trypsinized using 0.05% trypsin (Gibco) and seeded in 96- or 6-well (as per experiment) flat-bottomed plastic plates (Costar) for all assays. Tetrazolium salt, 3-4,5 dimethylthiazol-2,5-diphenyl tetrazolium bromide (MTT), DMSO, and paraformaldehyde were obtained from Sigma. Phalloidin conjugated to Alexa 594 was obtained from Molecular Probes (Invitrogen) and fluoromount from Souther Biotech.

General Procedures

NMR spectra were recorded using 400 MHz Jeol NMR spectrometer in $CDCl_3$ (for PDP-ester, CAR-ester) and DMSO-d_6 (for PDP-acid, CAR-acid, and all DEX-derivatives) containing a small amount of TMS as internal standard. FT-IR spectra of all compounds were recorded using Bruker αT Fourier transform infrared spectrometer. The mass of PDP and CAR derivatives were confirmed by using the Applied Biosystems 4800 PLUS MALDI TOF/TOF analyzer. High resolution mass spectra of PDP-acid cleaved from DEX-PDP were obtained from Micro Mass ESI-TOF MS spectrometer. The purity of the modified dextran were determined by gel permeation chromatography (GPC) using a Viscotek VE 1122 pump, Viscotek VE 3580 RI detector, and Viscotek VE 3210 UV/vis detector in dimethyl formamide. The absorption and emission studies were done by a Perkin-Elmer Lambda 45

UV–visible spectrophotometer and SPEX Fluorolog HORIBA JOBIN VYON fluorescence spectrophotometer with a double-grating 0.22 m Spex1680 monochromator and a 450 W Xe lamp as the excitation source at room temperature. The excitation spectra are collected at 375 and 420 nm (pyrene emission wavelength), and the emission spectra are recorded by exciting at the excitation maxima. The pyrene samples were purged with N_2 gas for at least 15–20 min prior to photophysical experiments. The size determination of the DEX-PDP, DEX-CAR, and DEX-SA were carried out by dynamic light scattering (DLS) using a Nano ZS-90 apparatus utilizing 633 nm red laser (at 90° angle) from Malvern Instruments. The reproducibility of the data was checked for at least three times using independent polymer solutions. The static light scattering experiment (SLS) was carried out using 3D-DLS spectrometer, from LS Instruments, Switzerland. The instrument consists of a He Ne laser having a wavelength of 632.8 nm attached to a computer using Lab view interface utilizing toluene as reference. The measurement was performed in autocorrelation mode from 20 to 130° by steps of 5°. Atomic force microscope (AFM) images were recorded by drop casting the samples on freshly cleaved mica surface, using Veeco Nanoscope IV instrument. The experiment was performed in tapping mode using TAP-190AL-G50 probe from Budget sensors with a nominal spring constant of 48 N/m and resonance frequency of 163.5. FE-SEM images were recorded using Zeiss Ultra Plus scanning electron microscope. For FE-SEM analysis, the samples were prepared by drop casting on silicon wafers and coated with gold. Thermal analysis of PDP-acid, CAR-acid, and stearic acid was performed using TA Q20 differential scanning calorimeter (DSC). The instrument was calibrated using indium standards. TEM images were recorded using a Technai-300 instrument by drop casting the sample on Formvar-coated copper grid. The fluorescent micrographs were collected using Carl Zeiss Axiovert 200 microscope. LSM710 confocal microscope was used for imaging the cells. The stability of CPT was analyzed by using reverse phase HPLC system, consists of Dionex ICS3000 instrument with phenomenix c18 reverse phase column (250× 4.60 mm) and UV detector, at flow rate of 1 mL/min. Single crystals were subjected to data collection at 100 K on Bruker APEX duo CCD-X-ray diffractometer equipped with graphite monochromated Mo Ka radiation (λ = 0.71073 Å). The frames were integrated with Bruker APEX software package. The structures were solved by direct methods and refined with a full matrix least-squares techniques using SHELX S v97 programs.

Synthesis of Ethyl 2-(3-Pentadecylphenoxy)acetate (PDP-Ester, 1a)

3-Pentadecylphenol (10.0 g, 32.8 mmol), K_2CO_3 (13.5 g, 98.5 mmol), and a pinch of KI were taken in dry dimethylformamide (50 mL) and stirred at 80 °C under a nitrogen atmosphere for 30 min. The content was cooled and ethyl chloroacetate (4.2 mL, 39.4 mmol) was added dropwise. The reaction continued by stirring at 80 °C for 24 h under a nitrogen atmosphere. The reaction mixture was poured into water (250 mL) and the product was extracted with ethyl acetate. The organic layer was washed with brine, dried over anhydrous sodium sulfate, and the solvent was removed to obtain the product as low melting solid. It was further purified by passing through a silica gel column using 3% ethyl acetate in hexane as eluent. Yield = 7.5 g (58%); mp = 38 °C. ^{1}H NMR (400 MHz, $CDCl_3$) δ 7.17 (t, 1H, Ar-**H**), 6.80 (d, 1H, Ar-**H**), 6.74 (s,1H, Ar-**H**), 6.69 (d, 1H, Ar-**H**), 4.59 (s, 2H, O-C**H$_2$**), 4.26 (q, 2H, O-C**H$_2$**-CH_3), 2.55 (t, 2H, Ar-C**H$_2$**), 1.48 (m, 2H, Ar-CH_2-C**H$_2$**), 1.28 (m, 27H, aliphatic-H), 0.87 (t, 3H,-C**H$_3$**). ^{13}C NMR ($CDCl_3$, 100 MHz) δ 169.34 (**C** = O), 158.10,

142.04, 129.72, 121.776, 115.01, 112.08 (Ar-**C**), 65.06 (Ar-O-**C**H_2), 61.07 (O-**C**H_2-CH_3), 35.68, 31.83, 31.42, 29.57, 29.41, 29.26, 22.63, and 14.48. FT-IR (KBr, cm^{-1}), 3037, 3006 (aromatic C–H stretch), 2925, 2854 (aliphatic C–H stretch), 1762 (ester C = O stretch), 1585 (ring C = C stretch), 1201 (C(= O)-O stretch). MALDI-TOF-TOF (MW: 390), *m/z* = 429 ($M + K^+$).

Synthesis of (*E*)-Ethyl 2-(3-Pentadec-7-enyl)phenoxy)-acetate (CAR Ester, 1b)

Cardanol (10.0 g, 33.0 mmol), K_2CO_3 (13.7 g, 99.0 mmol), KI, and ethyl chloroacetate (4.26 mL, 39.6 mmol) were reacted in dimethylformamide, as described for compound **1a,** and the product was obtained as a colorless liquid after column purification. Yield = 8.2 g (63%). ^{1}H NMR (400 MHz, $CDCl_3$) δ 7.17 (t, 1H, Ar-**H**), 6.80 (d, 1H, Ar-**H**), 6.75 (s, 1H, Ar-**H**), 6.70 (d, 1H, Ar-**H**), 5.34 (m, 2H, vinylic protons), 4.60 (s, 2H, O-C**H**$_2$), 4.26 (q, 2H, O-C**H**$_2$-CH_3), 2.56 (Ar-C**H**$_2$), 1.99 (C**H**$_2$-CH = CH-C**H**$_2$), 1.58 (m, 2H, Ar-CH_2-C**H**$_2$), 1.27 (m, 19H, aliphatic protons), 0.87 (t, 3H, aliphatic terminal C**H**$_3$). ^{13}C NMR ($CDCl_3$, 100 MHz) δ 169.28 (-C = O), 158.12, 144.45, 129.67, 121.68, 114.98, 112.02 (Ar-**C**), 130.48, 130.02 (vinylic **C**), 65.05 (Ar-O-**C**H_2), 61.04 (O-**C**H_2-CH_3), 35.69, 31.70, 31.68, 31.38, 29.65, 29.16, 27.13, 22.77, 22.64, 14.52 (aliphatic **C).** FT-IR (KBr), cm^{-1}), 3104, 3035 (aromatic C–H stretch), 2925, 2854 (aliphatic C–H stretch), 1764 (ester C = O stretch), 1654 (C = C stretch of long tail), 1585 (ring C = C stretch), 1201 (C(= O)-O stretch). MALDI TOF-TOF, (MW: 388), ***m/z*** = 427 ($M + K^+$).

Synthesis of 2-(3-Pentadecylphenoxy) Acetic Acid (PDP-Acid, 2a)

PDP-ester (5.0 g, 11.6 mmol) and KOH (2.2 g, 36.5 mmol) were taken in dioxane (50.0 mL) and refluxed for 24 h. After removal of dioxane, the solid content was dissolved in water (100 mL) and the unreacted PDP-ester was removed by extracting into ethyl actetate. The aqueous solution was acidified with dilute hydrochloric acid until the content became pH = 4. The precipitate was extracted with 50 mL of ethyl acetate, washed with water, and dried over anhydrous sodium sulfate. The solvent was removed to obtain the product as white solid which was further purified by passing through silica gel column using 20% ethyl acetate in hexane as eluent. Yield = 2.8 g (60%). ^{1}H NMR (400 MHz, d_6 DMSO) δ 12.9 ppm (s, 1H, CO-O**H**), 7.13 ppm (t, 1H, Ar-**H**), 6.67 ppm (m, 3H, Ar-**H**), 4.58 ppm (s, 2H, O-C**H**$_2$), 2.49 ppm (t, 2H, Ar-C**H**$_2$), 1.48 ppm (m, 2H, Ar-CH_2-C**H**$_2$), 1.28 ppm (m, 27H, aliphatic protons). ^{13}C NMR (DMSO-d_6, 100 MHz) δ 170.79 (CO–OH), 158.23, 144.46, 129.66, 121.52, 115.00, 111.90 (Ar-**C**), 64.83 (O-**C**H2), 35.68, 31.83, 31.46, 29.57, 29.26, 22.63, 14.48 (aliphatic-**C**). FT-IR (KBr, cm^{-1}) 3093, 3043 (aromatic C–H stretch), 2956, 2919, 2848 (aliphatic C–H stretch), 1731 (acid C = O stretch), 1577 (ring C = C stretch), 1421 (O–H bending), 1272 (C (=O)-O stretch). MALDI TOF-TOF, (MW: 362.5), *m/z* = 401.5 ($M + K^+$).

Synthesis of 2-(3-Pentadec-7-enyl)phenoxy)acetic Acid (CAR-Acid, 2b)

Compound CARD-ester (5 g, 11.7 mmol) was hydrolyzed using KOH (2.16 g, 38.65 mmol) in dioxane, as described for PDP-acid. Yield = 3.1g (67%). ^{1}H NMR (400 MHz, DMSO-d_6) δ12.9 (s, 1H, COO**H**), 7.19 (t, 1H, Ar-**H**), 6.83 (d, 1H, Ar-**H**), 6.76 (s, 1H, Ar-**H**), 6.71 (d, 1H, Ar-**H**), 5.33 (m, 2H, vinylic protons), 4.66 (s, 2H, O-C**H**$_2$), 2.56 (Ar-C**H**$_2$), 2.00 (C**H**$_2$-

CH = CH-C**H**$_2$), 1.58 (m, 2H, Ar-CH$_2$-C**H$_2$**), 1.27 (m, 19H, aliphatic protons), 0.87 ppm (t, 3H, aliphatic terminal C**H$_3$**). ^{13}C NMR (CDCl$_3$, 100 MHz) δ 170.77 (-C = O), 158.25, 144.45, 129.65, 121.51, 115.01, 111.91 (Ar-**C**), 130.57, 130.14 (vinylic **C**), 64.86 (Ar-O-**C**H$_2$), 35.68, 32.46, 31.67, 31.39, 29.63, 29.21, 27.10, 22.74, 22.62, 14.45 (aliphatic **C**). FT-IR (KBr), cm^{-1}) 3380 (O–H stretch), 3093, 3043 (aromatic C–H stretch), 3006 (alkene C–H stretch), 2956, 2921, 2850 (aliphatic C–H stretch), 1733 (acid C = O stretch), 1654 (C = C stretch of long tail), 1577 (ring C = C stretch), 1423 (O–H bending), 1272 (C (= O)-O stretch). MALDI TOF-TOF, (MW: 360), *m/z* = 399 (M + K$^+$).

Synthesis of DEX-PDP-*x*

Dextran (M_w = 6000, 1.0 g, 6.2 mmol of anhydroglucose unit) and compound **1b** (2.2 g, 6.2 mmol, for DEX-PDP-10) were dissolved in anhydrous DMSO (50.0 mL) and the solution was purged with dry nitrogen. 4-(Dimethylamino) pyridine (0.15 g, 1.24 mmol) in anhydrous DMSO (3.0 mL) and dicyclohexylcarbodiimide (1.53 g, 7.45 mmol) in anhydrous DMSO (3.0 mL) were added. The reaction mixture was stirred for 1 h at 25 °C and the reaction was continued at 80 °C for 24 h. The solution was cooled, filtered to remove dicyclohexyl urea, and the solvent was removed under reduced pressure. The thick viscous liquid was precipitated by adding into cold methanol (100 mL). The solid was filtered and washed several times with methanol. It was dissolved again in DMSO and the purification via the precipitation technique was done at least twice. The product filtered out and dried under vacuum at 60 °C to get yellowish white solid as product. Yield = 60%. ^{1}H NMR (400 MHz, DMSO-d_6) δ 7.12 (s, 1H, Ar-H), 6.72 (m, 3H, Ar-H), 4.47, 4.82, 4.88 (s, hydroxyl of dextran), 4.63 (s, dextran anomeric proton), 3.14–3.69 (dextran glucosidic protons), 2.49 (2H, Ar-C**H**$_2$), 1.48 (2H, Ar-CH$_2$-C**H$_2$**), 1.18–0.80 ppm (aliphatic protons). ^{13}C NMR (DMSO-d_6, 100 MHz) δ 168.95 (ester **C** = O), 158.2,144.52, 129.70, 121.69, 115.48, 111.80 (Ar-**C**), 98.69 (dextran anomeric **C**), 73.81, 72.33, 70.85, 70.58, 66.52 (dextran glucosidic carbons), 64.95 (O = C-**C**H2), 35.64, 31.81, 31.39, 29.55, 29.22, 25.19, 22.61, 14.49 (aliphatic carbons). FT-IR (KBr, cm^{-1}) 3376 (O–H stretch), 2920, 2852 (aliphatic C–H stretch), 1766 (ester C = O stretch), 1585 (ring C = C stretch), 1453 (O–H bending), 1198 (C (=O)-O stretch).

Synthesis of DEX-CAR-*x*

Dextran (M_n = 6000, 1 g, 6.1 mmol of anhydroglucose unit), compound **2b** (2.23 g, 6.1 mmol, for DEX-CAR-10), 4-(dimethyl amino)pyridine (0.15 g, 1.24 mmol), and dicyclohexylcarbodiimide (1.53 g, 7.45 mmol) were reacted in dry DMSO, as described for DEX-PDP-*x*. Yield = 60%. ^{1}H NMR (400 MHz, DMSO-d_6) δ 7.11 (s, 1H, Ar-H), 6.71 (m, 3H, Ar-H), 5.26 (vinylic protons), 4.45, 4.80, 4.86 (s, hydroxyl of dextran), 4.62 (s, dextran anomeric proton), 3.11–3.70 (dextran glucosidic protons), 2.48 (2H, Ar-C**H**$_2$), 1.92 (C**H**$_2$-CH = CH-C**H**$_2$), 1.48 (2H, Ar-CH$_2$-C**H$_2$**), 1.20–0.79 (aliphatic protons). ^{13}C NMR (DMSO-d_6, 100 MHz) δ 168.95 (ester, **C** = O), 158.2, 144.50, 129.68, 121.65, 115.50, 111.80 (Ar-**C**), 98.71 (dextran anomeric, **C**), 73.82, 72.34, 70.87, 70.60, 66.54 (dextran glucosidic carbons), 64.95 (O = C-**C**H2), 35.65, 31.83, 31.39, 29.57, 29.24, 27.11, 25.19, 22.62, 14.46 (aliphatic carbons). FT-IR (KBr, cm^{-1}) 3380 (O–H stretch), 3045, 3003

(aromatic C–H stretch), 2922, 2854 (aliphatic C–H stretch), 1762 (ester C = O stretch), 1582 (ring C = C stretch), 1453 (O–H bending), 1198 (C(=O)-O stretch).

DEX-PDP-*x* and DEX-CAR-*x* with various degrees of substitution were obtained by changing the mole ratios of PDP-acid to dextran as 0.5, 1.0, and 3.0 in the feed and their details are given in the Supporting Information. DEX-SA with a degree of substitution of 7.0 was synthesized using similar procedure as described for DEX-PDP-*x* with a mole ratio of stearic acid (SA) to dextran as 0.5 in the feed.

Preparation of DEX-Vesicles and Critical Vesicular Concentration (CVC)

DEX-PDP or DEX-CAR or DEX-SA (20 mg) was dissolved in DMSO (3.0 mL) and distilled water (3.0 mL) was added dropwise into the polymer solution with stirring at 25 °C. The resulting suspension was dialyzed against distilled water using commercial cellulose ester semipermeable membrane (SPECTRA/POR, MWCO 3500) for 24 h. The critical vesicular concentration (CVC) was determined using pyrene as a fluorescence probe. A predetermined amount (0.6 μM) of pyrene prepared in acetone was pipetted into 5 mL glass sample vials and then acetone was allowed to evaporate completely. DEX-PDP or DEX-CAR solutions at different concentration, varying from 6.2×10^{-7} to 3.1×10^{-3} M were added under the nitrogen purge to the vial containing pyrene and equilibrate for overnight. The excitation wavelength was set at 337 nm, the excitation slit at 3 nm, and the emission slit at 5 nm. For pyrene emission spectra, the ratio of fluorescent intensity at 375 and 386 nm was calculated and plotted against logarithm concentration of polymer concentration. The CVC was estimated at a polymer concentration of onset of the increase in I_{375}/I_{386} ratio.

Encapsulation of Hydrophilic Rhodamine-B and Loading Efficiency

The ability of aggregates to stabilize the water-soluble molecules in the inner aqueous compartment was checked using rhodamine B, Rh-B. Typically, 20 mg polymer conjugates and 2 mg rhodamine B were dissolved in 3 mL of DMSO and distilled water (3.0 mL) was added dropwise into the polymer solution with stirring at 25 °C. This solution was stirred for 12 h and then extensively dialyzed (SPECTRA/POR, MWCO 3500) against water. The rhodamine B stabilization in DEX-PDP-5 was checked for 7days under dialysis. But in the case of DEX-CAR and DEX-SA, rhodamine B was completely leached out within 48 h of dialysis. DEX-PDP-5 solution contains entrapped rhodamine B was further made up to 10 mL. The absorbance of encapsulated rhodamine B was measured by diluting 100 μL of dialyzed solution to 3 mL using DMSO as solvent. The rhodamine B content and loading efficiency of polymer vesicles was determined from beers law using molar absorption coefficient of dye as 116000. The loading efficiency of Rh-B was determined as 1.80 wt %.

Encapsulation of Camptothecin and Drug-Loading Efficiency

Dialysis method was used to incorporate camptothecin in vesicles. Typically, 50 mg of DEX-PDP and 5 mg of CPT was dissolved in 5 mL of DMSO. Under moderate stirring distilled water (5 mL) was added dropwise to the above solution. After stirring for 1 h at room temperature, the solution was transferred to a dialysis bag (SPECTRA/POR, MWCO 3500) and dialyzed against deionized water for 24 h. The resulting solution was filtered to remove unencapsulated camptothecin, and lyophilized. To determine CPT loading content

and encapsulation efficiency, 3 mg of freeze-dried CPT loaded DEX-PDP was dissolved in 1.0 mL of DMSO. A total of 100 μL of this solution was diluted to 3.0 mL with DMSO and the absorbance at 365 nm was measured on UV–visible spectrophotometer. The amount of CPT encapsulated in the vesicles was determined using the molar extinction coefficient of CPT as 11250. Drug loading content (DLC) and drug loading efficiency (DLE) were calculated using following equations.

$$\mathrm{DLE}(\%) = \{\text{weight of drug in vesicles/weight of drug in feed}\} \times 100\,\%$$
$$\mathrm{DLC}(\%) = \{\text{weight of drug in vesicles/weight of drug loaded vesicles}\} \times 100\,\%$$

Stability of CPT Free Drug and CPT Encapsulated in DEX-PDP Vesicles

HPLC method was used to study the stability of free CPT and CPT encapsulated in DEX-PDP vesicles under physiological condition (pH 7.4 and 37 °C). The mobile phase was consisting of 23% acetonitrile and 77% triethylamine acetate buffer (pH 6.0). For free CPT, a stock solution of 100 μg/mL was prepared in DMSO and 1.5 mL of stock solution was mixed with 1.5 mL PBS and incubated in PBS at 37 °C. An aliquot of 100 μL was withdrawn at 0.5, 1, 2, 4, 8, and 24 h and mixed with 1.9 mL of PBS and immediately analyzed by HPLC to determine the ratio of carboxylate to lactone. For the CPT loaded vesicles, 3 mg of freeze-dried DEX-PDP-CPT samples were dispersed in 3 mL of PBS, taken in dialysis tube, and incubated at 37 °C on a rotary shaker. At various time intervals, 100 μL of suspension was withdrawn, dissolved in DMSO, appropriately diluted with PBS (pH 7.4), and then immediately analyzed by HPLC.

In Vitro Release Studies

Dialysis method was used to study the release profile of CPT and rhodamine from DEX-PDP vesicles. Briefly, 3.0 mg DEX-PDP vesicles encapsulated with CPT or rhodamine was dispersed in 3.0 mL of PBS and placed in a dialysis tube. The tube was immersed in 100 mL of PBS (pH 7.4) taken in a beaker and whole solution was incubated at 37 °C. At definite time intervals, 3.0 mL of solution was withdrawn and replaced with equal volume of fresh PBS. Absorbance of the each aliquot has been measured and amount of the CPT or rhodamine released were calculated using Beer’s law. Raw CPT release was done in a similar manner by dispersing free CPT in PBS (an amount equivalent in the encapsulated vesicles). Esterase assisted drug release studies were carried out by adding 10 U esterase enzyme into the dialysis bag.

Cell Viability Assay (MTT Assay)

To observe the effect of CPT and DEX-PDP-CPT, a cell viability assay was performed in wild-type mouse embryonic fibroblasts using the tetrazolium salt, 3-4,5 dimethylthiazol-2,5-diphenyl tetrazolium bromide (MTT). Wild-type mouse embryonic fibroblasts (1×10^3) were seeded per well in a 96-well plate (Corning, U.S.A.) in 100 μL of DMEM with 10% FBS (fetal bovine serum) and allowed to adhere for 24 h. Prior to drug treatment, medium from cells was aspirated and 0.05 μM CPT and DEX-PDP with encapsulated CPT required to achieve a final concentration 0.05 μM CPT were prepared. These were added to 100 μL of DMEM with FBS in which the cells were incubated. A blank control, DMEM with FBS in

the absence of cells, and an untreated control, cells with DMEM containing FBS, were used in each experiment. All control and treated experiment wells were in triplicate. Cells were incubated for 48 h without a change in medium, and after 48 h, drug containing medium was aspirated. Freshly prepared stock of MTT in sterile PBS (5 mg/mL) was diluted to 50 μg/mL in 100 μL of DMEM with FBS and added to cells. Cells were then incubated with MTT for 4 h at 37 °C. Medium with MTT was then aspirated from wells and the purple formazan crystals formed as a result of reduction of MTT by mitochondrial dehydrogenase enzyme from cells were dissolved in 100 μL of 100% DMSO (added per well). The absorbance from formazan crystals was immediately measured using microplate reader at 570 nm (Varioskan Flash) and is representative of the number of viable cells per well.

Values from the triplicates for each control and treated set were noted and their means used for calculations. If one value from the triplicate had deviated substantially from the other two, it was not considered in the mean calculations. If the triplicate values were all variable the experiment was not used in the final calculations. The mean of the absorbance values for the blank control samples was subtracted from the average of the untreated control and treated samples, respectively. The values thus obtained for the untreated control samples were equated to 100% and relative percentage values for CPT and DEX-PDP-CPT calculated accordingly. Percentage values thus obtained for CPT and DEX-CPT treated wells were subtracted from the untreated control (100%) to determine the percentage loss in cell numbers (relative to control). Results thus obtained from seven experiments were compiled and differences between CPT and DEX-PDP-CPT treatment statistically evaluated using a paired two tail *t*-test.

Cell Viability Assay (Crystal Violet Labeling of Cells)

Wild-type mouse embryonic fibroblasts were seeded in six-well plates (Corning, U.S.A.) at a density of 5×10^4 cells per well. After allowing the cells to adhere overnight, the culture medium (DMEM + 10% FBS) was removed and 2 mL of medium with 0.1 μM drug was added to each well. Appropriate amounts of free CPT and DEX-PDP with CPT were dissolved in PBS and diluted in medium to achieve the final CPT concentration of 0.1 μM. A blank control, DMEM with FBS in the absence of cells, and an untreated control, cells with DMEM containing FBS, were used in each experiment. Cells were treated for 48 h at 37 °C in a CO_2 incubator after which drug-containing medium was removed and the cells were rinsed once with PBS and fixed with 1 mL of 3.5% paraformaldehyde in PBS (15 min at room temperature). Each well was gently rinsed twice with PBS and 2 mL of 0.05% crystal violet in PBS was added for staining for 11 min at room temperature. The plates were then rinsed with PBS and allowed to dry inverted overnight. Crystal violet bound to the cells was dissolved in 100% DMSO and the absorbance, which is related to the number of adherent cells in the well, was measured using a microplate reader at 590 nm (Varioskan Flash). The absorbance of the blank control well was subtracted from all control and treated wells. Values thus obtained in the control untreated wells were equated to 100% and relative percentage values for CPT and DEX-PDP-CPT treated wells were calculated accordingly. Percentage values thus obtained for CPT and DEX-CPT treated wells were subtracted from the untreated control (100%) to determine the percentage loss in cell numbers (relative to control). Results thus obtained from four independent experiments were compiled and

differences between CPT and DEX-PDP-CPT treatment statistically evaluated using a paired two-tail *t*-test.

Cellular Uptake of CPT by Confocal Microscopy

Wild-type mouse embryonic fibroblasts (WT MEFs) were seeded at a density of 5×10^4 cells on flame-dried coverslips placed in 6 well plates containing DMEM medium with 10% FBS and incubated at 37 °C for 18 h. The cells were then exposed to required concentration of CPT alone, DEX alone, and CPT loaded DEX-PDP or rhodamine B loaded DEX-PDP vesicles (both dissolved in PBS) for 2 h in a CO_2 incubator at 37 °C. After incubation, drug-containing medium was aspirated from each well, and cells were washed twice with PBS (1 mL × 2) and fixed with 3.5% paraformaldehyde solution in PBS for 15 min at room temperature. The cells were washed twice with PBS (1 mL) and stained with phalloidin conjugated to Alexa 594 (Invitrogen) diluted 1:500 in 3% BSA solution in PBS. After 1 h incubation, at room temperature, in the dark, the excess dye was washed from the plate and cells were again gently rinsed with PBS. The coverslips were mounted on slides using fluoromount mounting medium (Southern Biotech) and dried overnight at room temperature in the dark. The cells were imaged using a LSM710 confocal microscope using the λ 405 nm (blue channel) and λ 568 nm (red channel) lasers.

Images thus obtained were opened in the Image J analysis software and the image for each channel was separated. Phalloidin stained cell images (red channel) were processed using the threshold plugin and the threshold set to fill up the entire area of the cell. A mask was then created to map the edge of the thresholded cell, which was then saved as a region of interest (ROI) in the ROI manager. This ROI was then imported into the blue channel image and used to mapping the periphery of the cell in this image. The intensity of fluorescence within this ROI (hence within the cell) was now measured, as was the area of the ROI (hence the cell). Measured intensity values were then divided by the area of the cell to get an arbitrary value representing the intensity per unit area of each cell. Similar measurements and calculation were done for CPT, DEX-PDP, and DEX-PDP-CPT treated cells. Values thus obtained in 10 or more cells for each treatment were analyzed and differences statistically evaluated using a paired two tail *t*-test.

Results and Discussion

The hydroxyl groups in dextran were substituted with renewable resource hydrophobic motif 3-pentadecyl phenol (PDP), cardanol (CAR), or stearic acid (SA), as shown in Scheme 1. PDP was functionalized with carboxylic acid group and then anchored to the dextran hydroxyl group (MW = 6000) using DCC/DMAP. The degree of substitution was varied by using different mole ratios of the PDP acids in feed. The polymers were purified by repetitive precipitation and subsequent dialysis using semipermeable membrane. Similarly cardanol was also modified as described for PDP and anchored in the dextran backbone. Commercial available SA was directly used for dextran modification. The gel permeation chromatograms (GPC) of the modified dextran showed monomodel distribution with respect to pure samples and they were completely devoid of starting materials (see Supporting Information, SF-1). The structure of the PDP-attached dextran (DEX-PDP) was confirmed

Europe PMC Funders Author Manuscripts

by NMR and FT-IR spectroscopic analysis. ^{1}H NMR spectrum (see Figure 2a) of the substituted dextran showed peaks at 6.50–7.30 ppm and 0.5–3.00 ppm for the PDP aryl and aliphatic protons, respectively. The protons from dextran units appeared at 3.00–5.00 ppm. 14a Upon the formation of ester linkage, the protons Ar-OC**H**$_2$-COO-DEX appeared at 4.64 ppm, which merged with the anomeric protons of dextran (see Figure 2a). Similarly in the ^{13}C NMR spectrum (see Figure 2b), the carbon atom Ar-O**C**H$_2$-COO-dex appeared at 64.5 ppm. All the protons and carbons in the structure were assigned with the help of 2D NMR-HSQC technique (see Supporting Information, SF2).

The degree of substitution (DS) was estimated by comparing the peak intensities of anomeric proton in dextran at 4.62 ppm with the PDP aryl protons at 7.2 ppm in the hydrophobic part. The degree of substitution in dextran versus feed revealed that the incorporation of PDP hydrophobic units in the dextran linearly increased with increase in their feed (see SF-3 and SF-4). FT-IR spectrum of PDP-acid showed distinct stretching band at 1730 cm^{-1} with respect to -C = O stretching frequency (see SF-5). Upon the formation of ester linkage between dextran and PDP units, the -C = O stretching frequency shifted to a higher wavenumber at 1765 cm^{-1}.14a Additionally, the free hydroxyl groups in the dextran were also showed broad peaks at 3400 cm^{-1} in DEX-PDP-5. Thus, both NMR and FT-IR analysis confirmed the formation of the expected structure. Similarly, the structures of cardanol and SA-substituted dextrans were also confirmed by NMR and FT-IR (see SF-6–8 for DEX-CAR). The samples were named as DEX-PDP-*x*, DEX-CAR-*x*, and DEX-SA-*x*, where *x* corresponded to the actual incorporation of hydrophobic units in the dextran backbone determined by NMR (whole numbers are used for simplicity).

The newly designed dextran derivatives had unique amphiphilic structure and they self-organized in water (also PBS) through hydrophilic and hydrophobic interactions. The amphiphiles were found to be easily dispersible in water (or PBS buffer) at ambient conditions and produced clear solution. Dynamic light scattering (DLS) analysis of DEX-PDP-*x* was carried out in PBS buffer and the histogram for DEX-PDP-5 is shown in Figure 3a (see SF-9 for DEX-PDP-10 and DEX-PDP-19). A good autocorrelation with respect to self-assembled structures having uniform size distribution of 120 nm was obtained. The average sizes of the vesicles increased with increase in the PDP substitution in dextran from 120 to 300 nm for DEX-PDP-*x* (see SF-9). HR-TEM images of DEX-PDP-5 (Figure 3b) confirmed that these self-organized objects were nothing but spherical shaped vesicles with an average diameter of 110 ± 10 nm (n = 50). The sizes of the TEM image of vesicles were almost identical to that of DLS data. Field emission scanning electron microscopic (FE-SEM) images of DEX-PDP-5 also confirmed the formation of spherical vesicles (see SF-10).

The vesicular structure of DEX-PDP-5 was further investigated by AFM in both phase image (see Figure 3e) as well as in height image (see Supporting Information, SF-11). The phase image relies upon the energy that is dispersed from the vesicular structure to the AFM tip. The diameter of the vesicles were obtained as 140 ± 10 nm which matched with HR-TEM and DLS data (Figure 3a,b). In typical vesicle geometry, center part of the structure was assumed to be softer than peripheral region and the elevated phase was an indication of harder structures and vice versa (see Figure 3e).17a This surface difference in the vesicular

self-assembly dissipated the different responses to the force of AFM tip.17b The AFM images provide proof for the vesicular structure of the DEX-PDP-5. Static light scattering (SLS) technique was further employed to analyze the vesicular structure of the dextran polymer. Typically, in SLS technique the variation of scattered light intensity with its scattering angle was exploited to measure the size of a particle and determines the radius of gyration (R_g) of polymer structures in solution. The SLS data for DEX-PDP-5 in PBS at 25.0 ± 0.1 °C was carried out and the intensity of scattered light at different angle was plotted against q^2, where q is scattering vector magnitude (Guinier plot). The radius of gyration (R_g) was calculated from the slope of Guinier plot which was equivalent to $(R_g)^2/3$ (see Figure 3f, the detail calculation for the determination of R_g was provided in the Supporting Information, SF-12). The hydrodynamic radius (R_h) of the dextran polymer derivative thus obtained by the dynamic light scattering data was 60 nm (see Figure 3a, typically one measures the hydrodynamic diameter and half of this value is R_h). The R_h was determined from the plot in Figure 3a as 60 nm. The ratio of R_g/R_h if determined will directly provide the information on the solution assemblies of the polymer: $R_g/R_h = 0.77$ for hard spheres, $R_g/R_h = 1$ for vesicles, and $R_g/R_h = 1.7$ for coil-like structures.9,18 Adopting the above methodology and using the SLS and DLS data (based on the detail calculation, see Supporting Information, SF-12), the R_g/R_h value for the dextran polymer assemblies was determined to be $R_g/R_h = 1$. This provides evidence for the existence of vesicular structures, as observed in the HR-TEM and AFM images (see Figure 3).

DLS histograms and the HR-TEM image of DEX-CAR-5 also confirmed the formation of vesicles of 90 nm in diameter (see Figure 3c,d). The stearic acid substituted dextran derivative DEX-SA-7 showed the formation of small aggregates of 25 nm in the DLS (see SF-13). HR-TEM image of the DEX-SA-7 resembled as nanoparticle12a (see SF-14) rather than hollow vesicles as observed in the dextran modified with renewable resource hydrophobic tails (see Figure 3b,d). This provides evidence that the nature of the hydrophobic segments played a crucial role in determining the size and shape of the vesicular self-assemblies in dextran backbone. Interestingly, in the present investigation, the renewable resource hydrophobic units PDP and CAR were capable of producing exclusively vesicular shapes. PDP and CAR with a degree of substitution of 10% in the dextran backbone produced vesicles, and their TEM images are given in the Supporting Information, SF-15. However, the samples with 15–20% degree of substitution were found to be partially soluble in water for self-organization. The reasons for the renewable resource hydrophobic units directing the dextran backbone toward vesicular self-assemblies were analyzed based on two independent methods: (i) resolving the single crystal structures for the PDP units and (ii) thermal analysis of hydrophobic units to measure their degree of packing. To trace the nature of the chain packing in the vesicular structures, single crystal X-ray structure of the PDP acid was resolved (see Supporting Information). Crystals were grown for PDP acid in dichloromethane/acetone and its unit cell structure and other details are given in the Supporting Information (ST-1, SF-16 and SF-17). Based on the crystal structure, it could be concluded that the dextran vesicles were typically unilamellar in nature. Differential scanning calorimetry (DSC) thermograms of the hydrophobic units were recorded in heating/cooling cycles to understand their chain packing abilities (see Figure SF-18 and Table ST2). The enthalpies of the crystallization (ΔH_c) and melting transitions (ΔH_m) of the

PDP acid were obtained as ΔH_c = 49.5 kJ/mol and ΔH_m = 52.8 kJ/mol, respectively. The enthalpies of the stearic acid were found to be almost similar to that of PDP acid (ΔH_c = 47.7 kJ/mol and ΔH_m = 54.2 kJ/mol). Despite both PDP acid and stearic acid have similar enthalpy values (percentage of crystallinity), they showed a large difference in their self-organization in the dextran backbone (PDP acid produced vesicles and SA-induced nanoparticles). This was attributed to the lack of chain interpacking, as observed from the SA crystal structures.19 On the other hand, in PDP acids, the alkyl chains were interdigitized along the *c*-axis, as seen in their crystal packing (see SF17). Hence, it may be concluded that the strong interdigitations of the chains in the renewable resource hydrophobic tails facilitated the vesicular structures. This is the first time that such a good correlation has been established between the polysaccharide vesicles and their chemical structure using single crystal structure. The unsaturated tail molecule CAR acid showed less packing with lower energy terms (ΔH_c = 17.9 kJ/mol and ΔH_m = 23.3 kJ/mol) compared to that of its saturated counterpart. Typically, strongly packed chains showed higher crystallinity, needed higher energy for melting, and released more heat during crystallization. It confirmed that the unsaturated chains could be packed relatively weak in the DEX-CAR-*x* vesicles compared to that of DEX-PDP-*x* vesicles.

To study the stability of these vesicles, control experiments were carried out at various pH and long storage period. The vesicles were found to be stable for a long duration (3 days) and also in wide pH ranging from 4.0 to 9.2 (see SF-19). It confirmed that the vesicles were stable in both acidic and basic medium. The critical vesicular concentrations of the vesicles (CVCs) were determined using pyrene as fluorophore (see SF-20 to SF-22). A fixed pyrene amount (0.6×10^{-6} M) was encapsulated in the amphiphilic polymer scaffolds and subjected to photoexcitation using monochromatic light at 337 nm.20 Upon increasing the concentration of amphiphilic DEX-PDP scaffold in aqueous medium, pyrene molecules got encapsulated in the hydrophobic layer of the vesicles. Based on the pyrene fluorescence peak characteristics I_1/I_3 ratio (375/386 nm),20 the CVC of the DEX-PDP-5 and DEX-CAR-5 were determined as 6.2×10^{-5} M and 4.9×10^{-4} M, respectively (see SF-22). The concentration of the polymer samples were calculated based on the repeating unit mass of the anhydroglucose unit in dextran because the low degree of substitution of PDP (5%) does not contribute significantly to the concentration of the entire mass. The one order less concentration of CVC in DEX-PDP-5 confirmed the presence of strong packing of PDP units in their vesicular membranes compared to the unsaturated DEX-CAR-5 vesicles. This observation again supported the similar trend as seen in the DSC data for higher enthalpy values for PDP units with respect to a higher degree of packing. The precipitation of pyrene and polymer from the PBS hampered the CVC determination of the higher degree substituted dextran derivatives. This indicated that, at a higher degree of substitution, the encapsulation of polyaromatic molecules like pyrene in the unilamellar vesicles became almost impossible. Interestingly, less than 5% incorporation of PDP in dextran was sufficient enough to self-organize dextran backbone into stable vesicular assemblies.

One of the important experiments that could differentiate the nanoparticles from the vesicular assemblies is the encapsulation of the hydrophilic dyes (water-soluble dye, like Rhodamine B (Rh-B)) in the interior of the vesicles.21,22 Because the interior of the nanoparticle is hydrophobic, the encapsulations of water-soluble dyes do not occur. To

confirm the nature of these dextran assemblies, the derivatives DEX-PDP-5, DEX-CAR-5, and DEX-SA-7 were subjected to Rh-B encapsulation in water. The scaffolds and Rh-B were dissolved in DMSO + water and stirred for 12 h. Subsequently, the content was dialyzed in a semipermeable membrane for 48 h against water. The photographs are taken at regular intervals during the dialysis, which are shown in the Supporting Information (SF-23). The photographs of the Rh-B encapsulation are shown in Figure 4. The stability of the Rh-B was checked up to 7 days against dialysis in water and the results were almost the same. On the other hand, DEX-CAR-5 did not stabilize the Rh-B and only a faint amount got trapped (see Figure 4b). This suggests that unsaturated tailed layers did not produce stable vesicular structures for stabilizing water-soluble dye during dialysis. This observation was matching with DSC and CVC data for the packing of the tails in the saturated and unsaturated tails. As expected, the leaching out of Rh-B was faster in DEX-SA-7 due to its particle nature. The dialyzed sample vials were further exposed to photoexcitation using a hand-held UV-lamp (see Figure 4c). The photograph provided clear evidence for the presence of Rh-B (orange emission) in the encapsulated vesicles only in DEX-PDP-5. DLS histograms of the Rh-B encapsulated DEX-PDP-5 vesicles indicated that the vesicles were a little larger (170 nm, see Figure 4d) in size compared to the nascent vesicles (120 nm, see Figure 3a). HR-TEM image of DEX-PDP-5 (see Figure 4e) was found as solid spherical objects of 170 ± 10 nm with respect to the encapsulation of Rh-B in their vesicular interior compared to their nascent vesicles (see Figure 3b). The confocal microscope image of the Rh-B loaded vesicles also further confirmed their spherical shape and good luminescent in the encapsulated form (see Figure 4f). Further, the multiple acquisition analysis by fluorescence microscopy revealed that Rh-B was indeed occupied at the interior of the vesicles and not on the periphery (see SF-24). The AFM image (see SF-25) of the Rh-B loaded DEX-PDP-5 further proved the retention of the vesicular morphology. Further, the R_g/R_h was obtained as 1.11 based on the static light scattering (SLS) measurements in combination with DLS data (see SF-25), which again confirmed the existence of vesicular structures in the Rh-B loaded dextran vesicles. Thus, the custom designed DEX-PDP-5 vesicular structure is unique to encapsulate the water-soluble dye (Rh-B). These Rh-B vesicles were found to be stable under stored conditions for more than a month for further usage.

Anticancer drug camptothecin (CPT) was encapsulated in DEX-PDP-5 vesicles by dialysis method. The polymer to drug ratio was maintained as 10 wt % in the feed. The drug loading content was estimated using absorbance spectroscopy as 5.8 wt % in the vesicles (see Experimental Section for details). DLS histograms and features of the resultant drug-loaded dextran vesicle conjugate are shown in Figure 5. DLS analysis indicated (see Figure 5a) that the size of the drug–vesicle conjugate as 140 nm, which was almost similar to that of its nascent vesicle (120 nm, see Figure 3a). TEM images of drug–vesicle conjugate (see Figure 5b) confirmed the retaining of the spherical vesicular structure. The thin hydrophilic dextran as corona in the periphery was clearly evident from the expanded TEM image (see inset). Upon encapsulation of CPT in the hydrophobic sheet, the drug-loaded vesicle increased in size slightly from 110 nm to 120 ± 10 nm. The TEM image of the vesicles in the CPT loaded (or Rh-B loaded vesicles in Figure 4e) were different from the nascent hollow vesicles (see Figure 3b) due to the occupancy of the loaded molecules in the layer (or

interior). The AFM image of the CPT loaded dextran sample also showed the retention of the vesicular morphology (see SF-26). Further, the R_g/R_h ratio was also obtained as 1.11 (see SF-26) corresponding to the existence of a vesicular structure in the CPT loaded dextran vesicles. Typically, the camptothecin pharmacophore, α-hydroxylactone functionality, is highly susceptible for hydrolysis in PBS or blood plasma to its inactive carboxylic form (see Figure 5c).23 Therefore, it is important to quantify the active form of the encapsulated CPT in the DEX-PDP vesicles under the physiological condition at pH = 7.4 (in PBS). Both CPT loaded vesicle and CPT (alone) in PBS were incubated at 37 °C for 24 h. The samples were retrieved at regular interval and subjected to reverse phase HPLC for quantification of the CPT in its active form (see SF-27 and SF-28).24 CPT in carboxylic form (inactive form) and lactone form showed peaks at 7.2 and 19.2 min, respectively (see Figure 5c). From the HPLC traces it was evident that CPT in PBS underwent rapid hydrolysis from lactone to carboxylate, whereas the CPT loaded vesicles were preserved in the active form even after 8 h.

The percentage of active lactone form was plotted over the incubation time and the data were fitted with first order exponential drug hydrolysis [fit-values are given in the Supporting Information (SF-28-b, see also table ST3)]. In PBS, the hydrolysis of the drug was fast with $\tau_D = 2.6 \pm 0.9$ h and more than 96% of the CPT underwent fast decomposition into its inactive carboxylic acid form. On the other hand, the encapsulation of CPT in PDP-DEX-5 vesicles enhanced their stability as $\tau_D = 10.3 \pm 3.9$ h, which was four times better compared to the drug alone. The *Y*-intercepts (59.4%) revealed that more than 60% of the drug could be stabilized while encapsulated in the vesicles in PBS. Hence, the stability of CPT in vesicle was 10× higher than that of CPT in PBS alone (even after 24 h). Further, the CPT was found to be a fluorescent molecule due to the rigid aromatic core. The absorbance spectra of CPT (see Figure 5d) did not show any difference whether it was alone or encapsulated in vesicles. Upon photoexcitation (at excitation wavelength, 370 nm), the CPT showed deep blue emission and their emission maxima were varied with respect to its surrounding environment. The 10 nm red-shift in the emission spectra of CPT in PBS compared to CPT loaded vesicles was a clear indication of their stable form in the latter compared to former.25 The photograph of CPT drug-loaded vesicle (in PBS) showed the blue bright fluorescence (see figure 5d). The fluorescence microscope images of the same sample confirmed the existence of spherical objects with respect to their vesicular geometry (see SF-29). All the above studies confirmed that CPT was preserved in the active lactone form in the dextran vesicles.

The encapsulation of hydrophilic Rh-B and hydrophobic CPT were achieved in the interior and hydrophobic lamellar layer of the dextran vesicles through like–like interactions (for example, the hydrophobic layer has more preference for hydrophobic drug CPT loading and vice versa). Because these vesicular membranes were not cross-linked, the encapsulated molecules may be expected to release under dialysis over a period of time. Du et al.12a and Shen et al.26 had reported a more than 60% drug release in their un-cross-linked dextran nanoparticles and CPT-conjugated PEG vesicles, respectively. In the present case, the structures of the scaffolds were designed with aliphatic ester linkages between dextran and hydrophobic units. Hence, external stimuli such as esterase enzyme (abundant in cell cytoplasm) could also cleave the scaffold structures. Xu et al. had reported the estimation of

esterase enzyme in liver microsomes and cytosols in the range of 9.8–30.5 U.25 Alter et al. had reported that minimum of 10 U of esterase was required to cleave enzymatically polysaccharides derivaties.27b Based on these literature reports, 10 U of esterase was used to study the release behaviors of the in vitro release of CPT and Rh-B loaded vesicles either neat or in the presence of esterase (by dialyzing the at 37 °C). Aliquots were collected at regular intervals and they were subjected to absorption spectroscopy for the estimation of drug release. These experiments provided an opportunity to study the drug release from the vesicles either via natural leaching out under larger dilution or the chemical cleavage of the membrane layer by esterase. The plots of cumulative CPT or Rh-B release (%) over incubation time in the presence or in the absence of esterase are shown in Figure 6c. In the absence of enzyme, the scaffolds undergo natural leaching out of 60 ± 5% of the hydrophobic drug CPT within 5 h. In the presence of enzyme, the release processes happened in two steps: (i) initial rapid release of 60–70% of drug in 5 h and (ii) steady release of the remaining 30–40% of the drug over a period of 48 h. The faster drug release in the presence of esterase was correlated to its chemical action on the aliphatic-ester linkage that connects both the dextran and the hydrophobic PDP units (see Figure 6d).28 The photographs of the vials taken (see Figure 6a,b) in the presence of esterase clearly showed the precipitation (the precipitation occurred after 24 h) of samples with respect to the cleavage of vesicular membranes. In the absence of esterase, there was no precipitation (monitored up to one week) in the solution, indicating that the vesicular structures could partially disassemble, however, they did not precipitate from the aqueous medium. The chemical analysis of the precipitates by high resolution mass spectroscopy (HR-MS) confirmed the cleavage of PDP acid units from the dextran scaffolds (see HR-MS spectrum in SF-30). The PDP acid was nothing, but the renewable derivative was initially used for the functionalization of dextran and, therefore, is not expected to be toxic. Hence, based on these control experiments, it could be concluded that the custom-designed dextran vesicular structure was selective to cleave under esterase and release entire drugs under physiological conditions.

The in vitro release studies of Rh-B loaded vesicles (see Figure 6c) showed a similar release in the presence of the esterase enzyme. Up to 40 ± 5% of the Rh-B was released under similar conditions in 12 h and this release was enhanced up to 70 ± 2% in the presence of esterase. Surprisingly, the Rh-B release was not completed for the 10 U of esterase enzyme. This could be correlated to the difference in the activity of the esterase enzyme toward the hydrophilic Rh-B loaded dextran vesicles compared to that of the hydrophobic CPT loaded vesicles. To check this point, a control experiment was carried out under in vitro release using an excess amount of esterase (30 U; see Supporting Information, SF31). At higher enzyme concentration, the Rh-B loaded vesicle released all the Rh-B dye within 24 h. Interestingly, the present scaffold with Rh-B was found to show more stability toward the external stimuli such as esterase. The CPT or Rh-B loaded vesicles produced turbidity in the presence of esterase, which precipitated after 24 h. The natural release occurred only under the in vitro release studies at 37 °C during the prolonged dialysis against a large amount of water. The samples were found to be stable under storage conditions (at 4 °C, lyophilized dried sample in a vial or Rh-B vesicles in solution in the refrigerator). The unique

advantages of the present design are that the scaffold could encapsulate both hydrophilic and hydrophobic guest molecules.

Cytotoxicity of the polymer vesicle and its drug conjugate were tested on wild type mouse embryonic fibroblasts cells (WTMEFs) using the MTT assay.29 Cytotoxicity of the polymer vesicles for 0.05 and 1.87 μM in PBS (see Figure 7a) was found to be nontoxic to fibroblasts at both concentrations. Under identical conditions, 0.05 μM of CPT in PBS and CPT encapsulated vesicles in PBS when tested showed an ~2-fold increase in loss of viable cell numbers (detected using a crystal violet staining of cells, see SF-32 and SF-33)30 and an ~2.5-fold increase in cytotoxicity (detected by the MTT assay, see Figure 7b) by CPT in vesicle as compared to CPT alone in PBS. Thus, CPT loaded dextran vesicle was indeed more effective in killing cells than the drug alone. To visualize the cellular uptake of the drug–vesicle conjugate, the treated MEFs were analyzed by confocal microscope (Figure 7c). WTMEFs were treated with 35 μM concentration of either CPT alone or CPT loaded vesicles or an equivalent amount of DEX-PDP-5 without CPT for 2 h. This concentration of CPT was selected based on the ability to detect its fluorescence in cells using the λ 403 nm laser in the confocal microscope (see Figure 7c). Cells were also stained with phalloidin conjugated to Alexa dye, which specifically binds F-actin and labels the actin cytoskeletal network in cells. This staining was visualized using a 568 nm laser and was used to define the morphology of the adherent spread cell (see Figure 7c). No major changes in morphology or actin cytoskeletal organization of cells were detected in the time the cells were treated. Phalloidin staining of cells was also used to map the spread area of individual cells to measure total CPT fluorescence in cells using the Image J software.

Intensity thus calculated and equated to the area of the cell showed a significant increase in CPT fluorescence in cells treated with CPT loaded DEX-PDP-CPT vesicles as compared to CPT or DEX-PDP alone (see Figure 7c). CPT alone at the high 35 μM concentration was seen to also form aggregates that were seen to be deposited on the coverslip as bright fluorescent spots (see Figures 7c and SF-29). This was not observed in CPT loaded in DEX-PDP vesicles (see Figure 7c). Careful analysis of the confocal images showed the presence of fluorescent CPT (observed at 403 nm) in distinct vesicles localized in the perinuclear region (marked by solid white arrows; see Figure 7d). The nucleus in a representative cell is marked with a dotted line and labeled as “N”. These results confirmed the cellular uptake of the dextran vesicles and their localization in cells.

The ability of the DEX-PDP-5 scaffold to deliver hydrophilic molecules into cells was checked by analyzing the cellular uptake of Rh-B. This hydrophilic dye molecule exhibits a strong emission at 580 nm, enabling a direct visualization inside the cell. MEFs were hence treated with 200 μM DEX-PDP-5 containing Rh-B for 2 h and analyzed by confocal microscope using the (λ = 568 nm) laser (Figure 8a). This concentration of DEX-PDP-Rh-B was selected based on the ability to detect its fluorescence and hence uptake and localization in cells. Cells were also stained with phalloidin conjugated to Alexa 488 dye that specifically binds F-actin and labels the actin cytoskeletal network in cells. This staining was visualized using a 488 nm laser and was used to define the morphology of the adherent spread cell (see Figure 8a). DEX-PDP-Rh-B was seen to localize in vesicular structures (of μm to sub-μm size) that showed distinct perinuclear localization. Mouse fibroblasts were

further treated with 200 μM concentration for increasing times (2 and 24 h) and the uptake of DEX-PDP-Rh-B was compared. As described earlier, phalloidin staining of cells was used to map the spread area of individual cells and the red florescence in cells measured using the Image J software. Intensity thus calculated and equated to the area of the cell showed a significant increase in rhodamine fluorescence in cells treated for 24 h versus 2 h, both of which were significantly higher than the control (Figure 8b). This suggests that uptake of the DEX-PDP vesicles is rapid but also sustained showing an ~25% increase after the first 2 h leading up to 24 h. Moreover, these studies suggest that the integrity of the scaffold is retained inside the cells as rhodamine fluorescence was seen localized in distinct vesicular structures. Disruption of the integrity of the scaffold would have resulted in release of rhodamine and its dispersion in the cytosol of the cell. Ongoing work is focused on identifying the subcellular compartment that these vesicles localize to and the endocytic pathway they use to enter the cell in normal and cancer cells.

Conclusion

In conclusion, dextran vesicles based on renewable resource starting materials were successfully designed and synthesized as a delivery vehicle for encapsulation of both hydrophobic anticancer drug camptothecin as well as water-soluble Rh-B molecules (or drugs). These newly synthesized dextran-PDP (DEX-PDP) amphiphilic polymers were self-assembled under physiological conditions as vesicles of ~120 nm in size. The vesicular assemblies of the dextram polymer were further confirmed by HR-TEM, AFM, dynamic, and static light scattering analysis. The vesicular structures efficiently encapsulated CPT in the unilamellar pocket and also retained the active lactone pharmacophore in CPT more than 10× better compared to CPT alone in PBS. The hydrophilic and hydrophobic segments in dextran vesicles were made up of aliphatic ester-linkage which was cleaved by esterase (as stimuli) for the large drug release under physiological conditions. In vitro drug release studies confirmed that the vesicular scaffolds with water-soluble dye (or drug) showed enhanced stability against esterase for more than 12 h. Cytotoxicity studies revealed that the polymer scaffold was nontoxic. The efficiency of the drug in killing the cells was found to be 2.5× better when encapsulated in the vesicles compared to CPT alone. Compared to free CPT, the drug loaded vesicles showed significantly better cellular uptake and were seen to localize in a perinuclear region in cells. Additionally, the dual loading capability of the dextran vesicles for both hydrophilic and hydrophobic guest molecules (or drugs) provide a new opportunity to study the combination of two drug loadings in a single nanoscaffold. The unique dextran vesicles are not only restricted to CPT delivery, but are currently being explored for loading other fluorescent markers and other anticancer drugs. Understanding the cellular uptake mechanism, delivery, and trafficking in normal and cancer cells is also being investigated.

Supporting Information

Refer to Web version on PubMed Central for supplementary material.

Acknowledgments

The authors thank research grant from Department of Science and Technology (DST), New Delhi, India, under Nanomission Initiative Project SR/NM/NS-42/2009. N.B. was supported by the Ramalingaswami fellowship from the Department of Biotechnology. N.B. lab is now supported by a Senior Fellowship grant from the Wellcome Trust DBT Alliance. K.T. was supported by fellowships from the Pelotonia International Fellowship Program and IISER, Pune, during her stay in the N.B. Lab as a Pelatonia Fellow. P.S.P. thanks IISER Pune for a research fellowship. The authors thank National Chemical laboratory, Pune, India, for HR-TEM, SLS, and AFM facilities.

References

(1). (a)Duncan R. Nat Rev Cancer. 2006; 6:688–701. [PubMed: 16900224] (b)Haag R, Kratz F. Angew Chem, Int Ed. 2006; 45:1198–1215.(c)Chang TMS. Nat Rev Drug Discovery. 2005; 4:221–235. [PubMed: 15738978]

(2). (a)Davis ME, Chen Z, Shin MD. Nat Rev Drug Discovery. 2008; 7:771–782. [PubMed: 18758474] (b)Liu S, Maheshwari R, Kiick KL. Macromolecules. 2009; 42:3–13. [PubMed: 21494423] (c)Xiong M, Bao Y, Yang X, Wang Y, Sun B, Wang J. J Am Chem Soc. 2012; 134:4355–4362. [PubMed: 22304702] (d)Ryu J, Chacko R, Jiwapanich S, Bickerton S, Prakash Babu R, Thayumanavan S. J Am Chem Soc. 2010; 132:17227–17235. [PubMed: 21077674] (e)Jiwapanich S, Ryu J, Bickerton S, Thayumanavan S. J Am Chem Soc. 2010; 132:10683–10685. [PubMed: 20681699]

(3). (a)Matsumura Y, Maeda H. Cancer Res. 1986; 46:6387–6392. [PubMed: 2946403] (b)Fang J, Nakamura H, Maeda H. Adv Drug Delivery Rev. 2011; 63:136–151.(c)Maeda H. Bioconjugate Chem. 2010; 21:797–802.

(4). (a)Rosler A, Guido WM, Klok H. Adv Drug Delivery Rev. 2001; 53:95–108.(b)Zhang L, Chan JM, Gu FX, Rhee J, Wang AZ, Aleksandar F, Moreno R, Alexis R, Langer R, Farokhzad OC. ACS Nano. 2008; 2:1696–1702. [PubMed: 19206374] (c)Qiu L, Bae Y. Pharm Res. 2006; 23:1–30. [PubMed: 16392022] (d)Soussan E, Cassel S, Blanzat M, Rico-Lattes I. Angew Chem, Int Ed. 2009; 48:274–288.(e)Klaikherd A, Nagamani C, Thayumanavan S. J Am Chem Soc. 2009; 131:4830–4838. [PubMed: 19290632] (f)Honga C, Le Meins J-F, Borsali R, Taton D, Gnanou Y. Chem Commun. 2007:3063–3065.(g)Carlmark A, Malmstrom E. Biomacromolecules. 2003; 4:1740–1745. [PubMed: 14606904] (h)Bontempo D, Masci G, De Leonardis P, Mannina L, Capitani D, Crescenzi V. Biomacromolecules. 2007; 7:2154–2161.

(5). (a)Discher BM, Won Y, Ege DS, Lee J, Bates FS, Discher DE, Hammer DA. Science. 1999; 284:1143–1146. [PubMed: 10325219] (b)Dimova R, Seifert U, Poulingy B, Forster S, Dobereiner HG. Eur Phys J E. 2002; 7:241–250.(c)Opsteen JA, Cornelissen JJLM, van Hest JCM. Pure Appl Chem. 2004; 76:1309–1319.

(6). (a)Brinkhuis RP, Rutjes FPJT, van Hest JCM. Polym Chem. 2011; 2:1449–1462.(b)Ben-Haim N, Broz P, Marsch S, Meier W, Hunziker P. Nano Lett. 2008; 8:1368–1373. [PubMed: 18444692] (c)Kita-Tokarczyk K, Grumelard J, Haefele T, Meier W. Polymer. 2005; 46:3540–3563.

(7). (a)Mizrahy S. Peer D Chem Soc Rev. 2012; 41:2623–2640. [PubMed: 22085917] (b)Schatz C, Lecommandoux S. Macromol Rapid Commun. 2010; 31:1664–1684. [PubMed: 21567580] (c)Smita K, Jayakannan M. J Phys, Chem B. 2012; 116:9820–9831. [PubMed: 22803511]

(8). (a)Discher DE, Eisenberg A. Science. 2002; 297:967–973. [PubMed: 12169723] (b)Discher DE, Ahmed F. Annu Rev Biomed Eng. 2006; 8:323–341. [PubMed: 16834559]

(9). Houga, Cm; Giermanska, J; Lecommandoux, Sb; Borsali, R; Taton, D; Gnanou, Y; Le Meins, J-FO. Biomacromolecules. 2009; 10:32–40. [PubMed: 19072234]

(10). (a)Tassa C, Shaw SY, Weissleder R. Acc Chem Res. 2011; 44:842–852. [PubMed: 21661727] (b)Mehvar R. J Controlled Release. 2000; 69:1–25.

(11). (a)Raemdonck K, Naeye B, Buyens K, Vandenbroucke RE, Hogset A, Demeester J, De Smedt SC. Adv Funct Mater. 2009; 19:1406–1415.(b)Raemdonck K, Thienen TGV, Vandenbroucke RE, Sanders NK, Demeester J, De Smedt SC. Adv Funct Mater. 2008; 18:993–1001.(c)Morais M, Subramanian S, Pandey U, Samuel G, Venkatesh M, Martins M, Pereira S, Correia JDG, Santos I. Mol Pharm. 2011; 8:609–620. [PubMed: 21299250]

(12). (a)Bachelder EM, Beaudette TT, Broaders KE, Dashe J, Fréchet JMJ. J Am Chem Soc. 2008; 130:10494–10495. [PubMed: 18630909] (b)Broaders KE, Cohen JA, Beaudette TT, Bachelder EM, Fréchet JMJ. Proc Natl Acad Sci USA. 2009; 106:5497. [PubMed: 19321415] (c)Keliher EJ, Yoo J, Nahrendorf M, Lewis JS, Marinelli B, Newton A, Pittet MJ, Weissleder R. Bioconjugate Chem. 2011; 22:2383–2389.

(13). Important references for modified-dextran: Stubbe BG, Horkey F, Amsden B, Hennink WE, De Smedt SC, Demeester J. Biomacromolecules. 2003; 4:691–695. [PubMed: 12741786] (b)Pescosolido L, Schuurman W, Malda J, Matricardi P, Alhaique F, Coviello T, van Weeren PR, Dhert WJA, Hennink WE, Vermonden T. Biomacromolecules. 2011; 12:1831–1838. [PubMed: 21425854] (c)Tomme SRV, Mens A, van Nostrum CF, Hennink WE. Biomacromolecules. 2008; 9:158–165. [PubMed: 18081253] Lee MH, Boettiger D, Composto RJ. Biomacromolecules. 2008; 9:2315–2321. [PubMed: 18686998] (d)Hiemstra C, van der Aa LJ, Zhong Z, Dijkstra PJ, Feijen J. Biomacromolecules. 2007; 8:1548–1556. [PubMed: 17425366] (e)Nagahama K, Mori Y, Ohya Y, Ouchi T. Biomacromolecules. 2007; 8:2135–2141. [PubMed: 17559263] (f)Matricardi P, Pontoriero M, Coveillo T, casadei MA, Alihaique F. Biomacromolecules. 2008; 9:2014–2020. [PubMed: 18558740] (g)Nielsen TT, Wintgens V, Amiel C, Wimmer R, Larsen KL. Biomacromolecules. 2010; 11:1710–1715. [PubMed: 20553039] (h)Ohya Y, Oue H, Nagatomi K, Ouchi T. Biomacromolecules. 2001; 2:927–933. [PubMed: 11710051] (i)Zhang H, Qadeer A, Chen W. Biomacromolecules. 2011; 12:1428–1437. [PubMed: 21410248] (j)Liebert T, Wostschadlo J, Laudeley P, Heinze T. Biomacromolecules. 2011; 12:3107–3113. [PubMed: 21739976]

(14). (a)Du Y-Z, Weng Q, Yuan H, Hu F-Q. ACS Nano. 2010; 4:6894–6902. [PubMed: 20939508] (b)Sun H, Guo B, Li X, Cheng R, Meng F, Liu H, Zhong Z. Biomacromolecules. 2010; 11:848–854. [PubMed: 20205476] (c)Goodwin AP, Tabakman SM, Welsher K, Sherlock SP, Prencipe G, Dai H. J Am Chem Soc. 2009; 131:289–296. [PubMed: 19061329] (d)Broaders KE, Grandhe S, Frechet JMJ. J Am Chem Soc. 2011; 133:756–758. [PubMed: 21171594] (e)Li Y-L, Zhu L, Liu Z, Cheng R, Meng F, Cui J-H, Ji S-J, Zhong Z. Angew Chem, Int Ed. 2009; 48:9914–9918. (f)Liebert T, Hornig S, Hesse S, Heinze T. J Am Chem Soc. 2005; 127:10484–10485. [PubMed: 16045324]

(15). Schatz C, Louguet S, Le Meins J-F, Lecommandoux S. Angew Chem, Int Ed. 2009; 48:2572–2575.

(16). (a)Anilkumar P, Jayakannan M. Macromolecules. 2007; 40:7311–7319.(b)Antony MJ, Jayakannan M. J Phys Chem B. 2011; 115:6427–6436. [PubMed: 21539329] (c)Anilkumar P, Jayakannan M. Macromolecules. 2008; 41:7706–7715.(d)Anilkumar P, Jayakannan M. J Phys Chem B. 2009; 113:11614–11624. [PubMed: 19642663] (e)Anilkumar P, Jayakannan M. J Phys Chem B. 2010; 114:728–736. [PubMed: 19924837] (f)Bhavsar GA, Asha SK. Chem—Eur J. 2011; 17:12646–12658. [PubMed: 21956257] (f)John G, Vemula PK. Soft Matter. 2006; 2:909–914.

(17). (a)Yang M, Wang W, Yuan F, Zhang X, Li J, Liang F, He B, Minch B, Wegner G. J Am Chem Soc. 2005; 127:15107–15111. [PubMed: 16248650] (b)Latrou H, Frielinghaus H, Hanski S, Ferderigos N, Ruokolainen J, Ikkala O, Richter D, Mays J, Hadjichristidis N. Biomacromolecules. 2007; 8:2173–2181. [PubMed: 17583949]

(18). Burchard W. Adv Polym Sci. 1983; 48:1–124.

(19). Malda V, Celotti G, Zannetti R, Martelli AF. J Chem Soc (B). 1971:548–553.

(20). (a)Winnik FM. Chem Rev. 1993; 93:587–614.(b)Kalyanasundaram K, Thomas JK. J Am Chem Soc. 1977; 99:2039–2044.(c)Keyes-Baig C, Duhamel J, Fung S-Y, Bezaire J, Chen P. J Am Chem Soc. 2004; 126:7522–7532. [PubMed: 15198599] (d)De Maria P, Fontana A, Siani G, D'Aurizio E, Cerichelli G, Chiarini M, Angelini G, Gasbarri C. Colloids Surf, B. 2011; 87:73–78.(e)Delample M, Jerome F, Barrault J, Douliez J-P. Green Chem. 2011; 13:64–68.

(21). Yan Q, Yuan J, Cai Z, Xin Y, Kang Y, Yin Y. J Am Chem Soc. 2010; 132:9268–9270. [PubMed: 20565093]

(22). (a)Yan Q, Zhou R, Fu C, Zhang H, Yin Y, Yuan J. Angew Chem Int Ed. 2011; 50:4923–4927. (b)Xu J, Tao l, Boyer C, Lowe AB, Davis T. Macromolecules. 2011; 44:299–312.(c)Koley P, Pramnanik A. Soft Matter. 2012; 8:5364–5374.(d)Du J, Armes SP. J Am Chem Soc. 2005; 127:12800–12801. [PubMed: 16159264]

(23). Venditto VJ, Simanek EE. Mol Pharm. 2010; 7:307–349. [PubMed: 20108971]

(24). Sano K, Yoshikawa M, Hayasaka S, Satake K, Ikegami Y, Yoshida H, Ishikawa T, Sawada S, Tanabe S. J Chromatogr, B. 2003; 795:25–34.

(25). di Nunzio MR, Cohen B, Douhal A. J Phys Chem A. 2011; 115:5094–5104. [PubMed: 21534546]

(26). Shen Y, Zhang B, Murphy CJ, Sui M, Zhao J, Wang J, Tang J, Fan M, Kirk EV, Murdoch WJ. J Am Chem Soc. 2010; 132:4259–4265. [PubMed: 20218672]

(27). (a)Xu G, Zhang W, Ma MK. Clin Cancer Res. 2002; 8:2605–2611. [PubMed: 12171891] (b)Alter SC, Metcalfe DD, Bradford TR, Schwartz LB. Biochem J. 1987; 248:821–827. [PubMed: 2449172]

(28). Burkhart DJ, Barthel BL, Post GC, Kalet BT, Nafie JW, Shoemaker RK, Koch TH. J Med Chem. 2006; 49:7002–7012. [PubMed: 17125253]

(29). Urasaki Y, Laco GS, Pourquier LP, Takebayashi Y, Kohlhagen G, Gioffre C, Zhang H, Chatterjee D, Pantazis P, Pommier Y. Cancer Res. 2001; 61:1964–1969. [PubMed: 11280753]

(30). (a)Gilbert NL, Magel TT, Lipkin D. J Am Chem Soc. 1942; 64:1774–1782.(b)Pichierri P, Franchitto A, Piergentili R, Colussi C, Palitti F. Carcinogenesis. 2001; 22:1781–1787. [PubMed: 11698339]

Europe PMC Funders Author Manuscripts

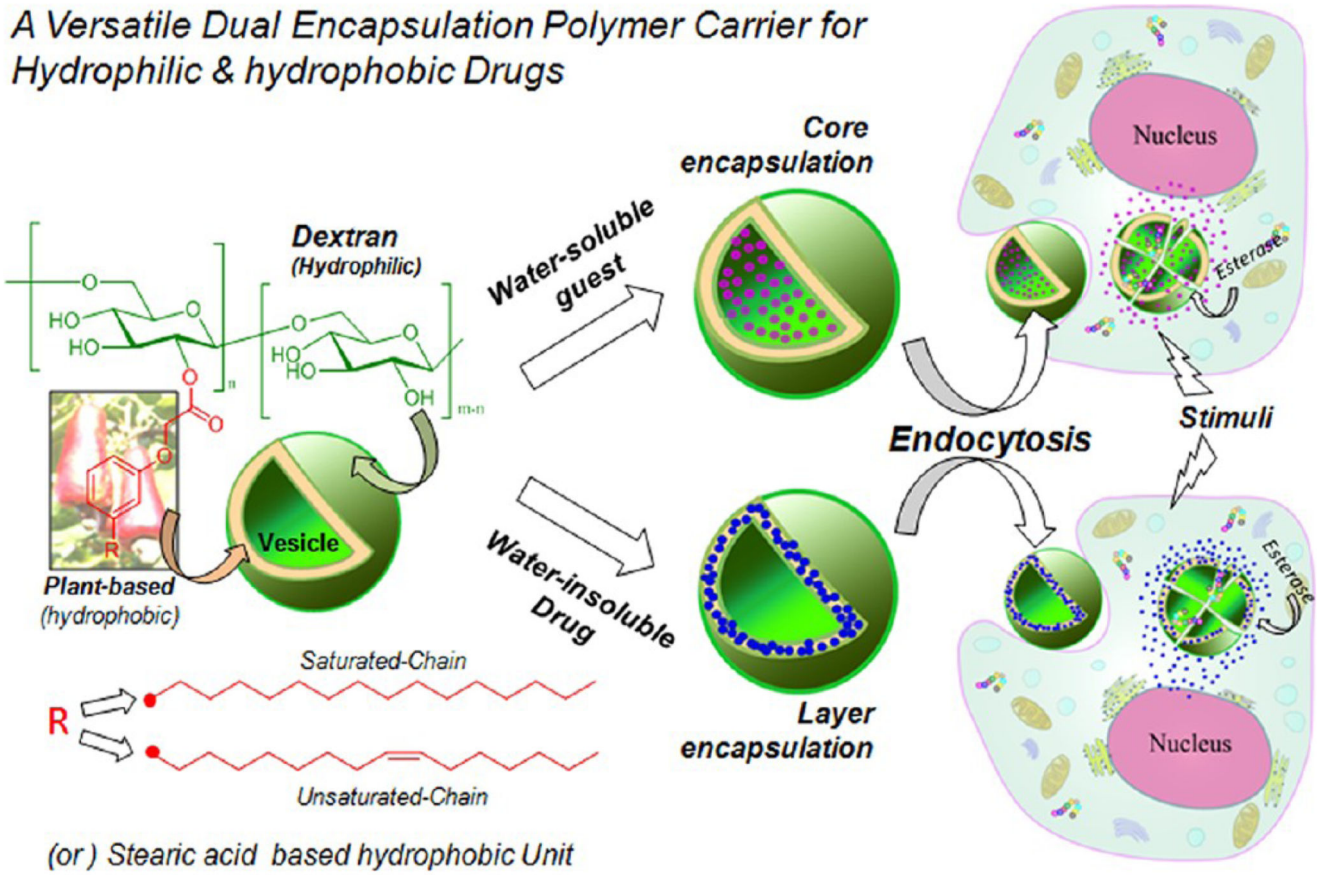

Figure 1.

Dextran vesicular approach for delivery of hydrophilic and hydrophobic drugs (or molecules) into cells.

Europe PMC Funders Author Manuscripts

Europe PMC Funders Author Manuscripts

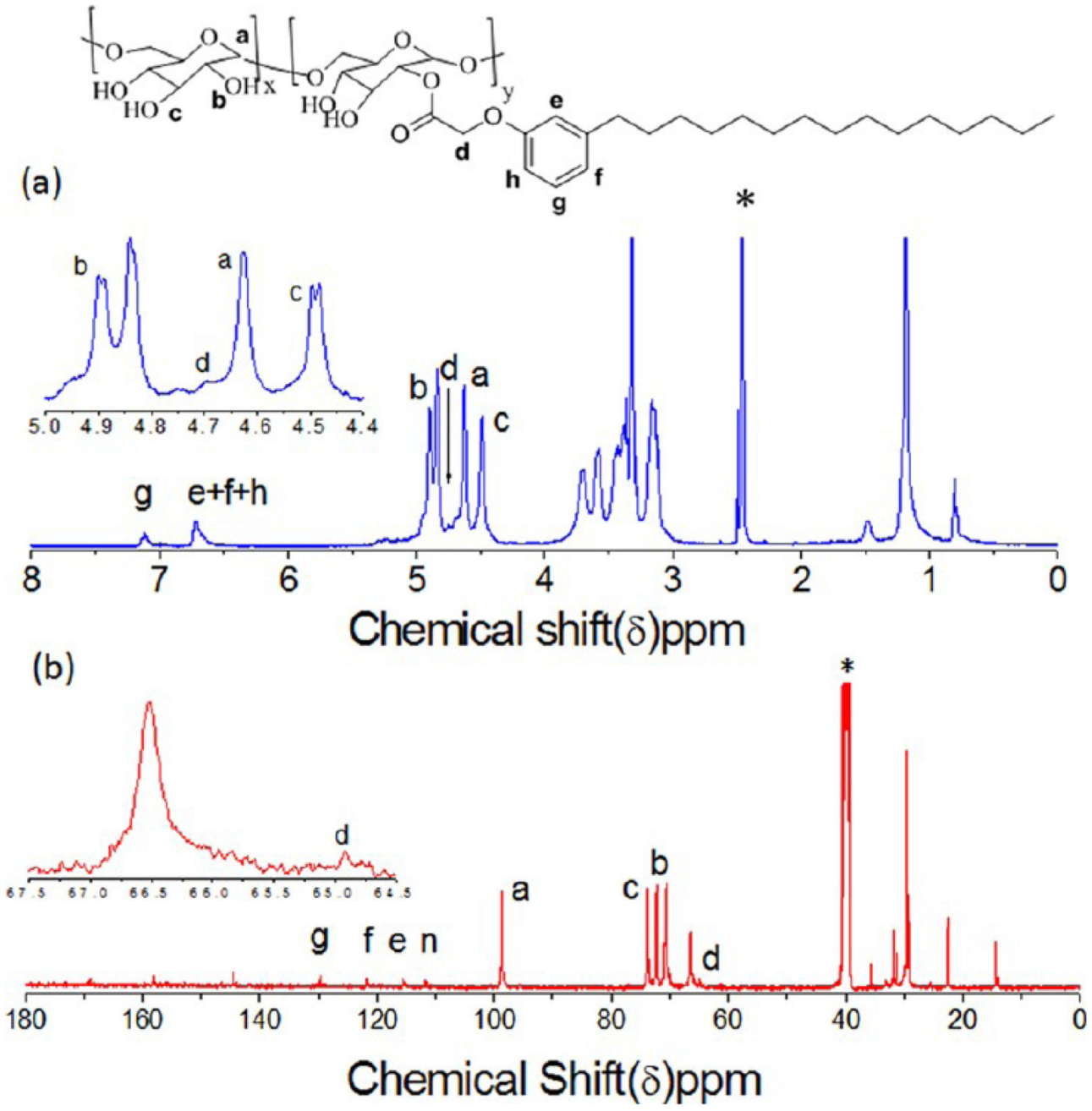

Figure 2.
^{1}H and ^{13}C NMR spectra of dextran-PDP amphiphilic polymers (in DMSO-d_6).

Europe PMC Funders Author Manuscripts

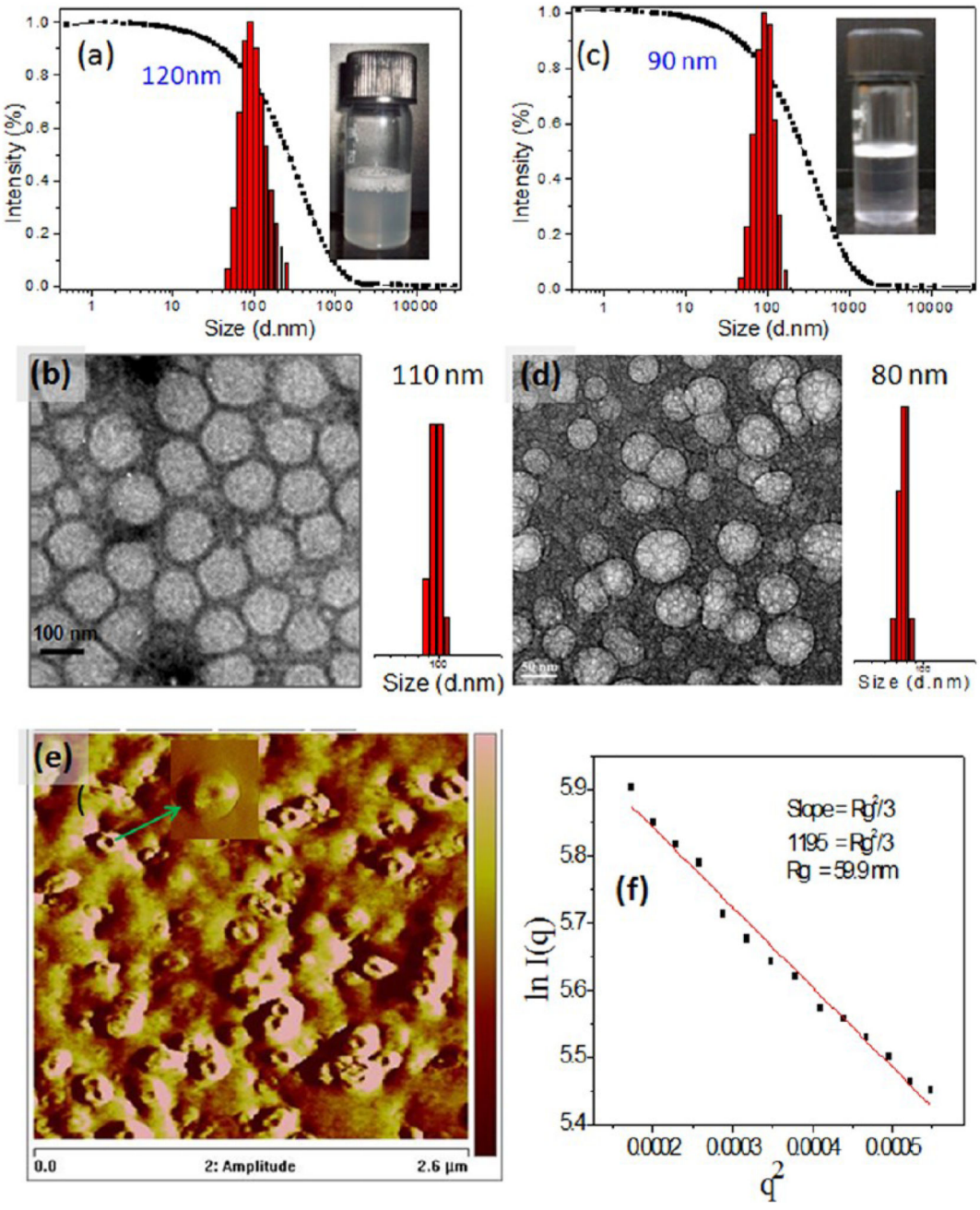

Figure 3.

DLS histogram (a) and HR-TEM (b) of DEX-PDP-5 in PBS. DLS histogram (c) and HR-TEM (d) of DEX-CAR-5 in PBS. (e) AFM phase images of DEX-PDP-5 vesicular structure. (f) Static light scattering data for DEX-PDP-5 in PBS at 25 °C (0.5 mg/mL). The vials showed the solution containing the vesicles in water.

Europe PMC Funders Author Manuscripts

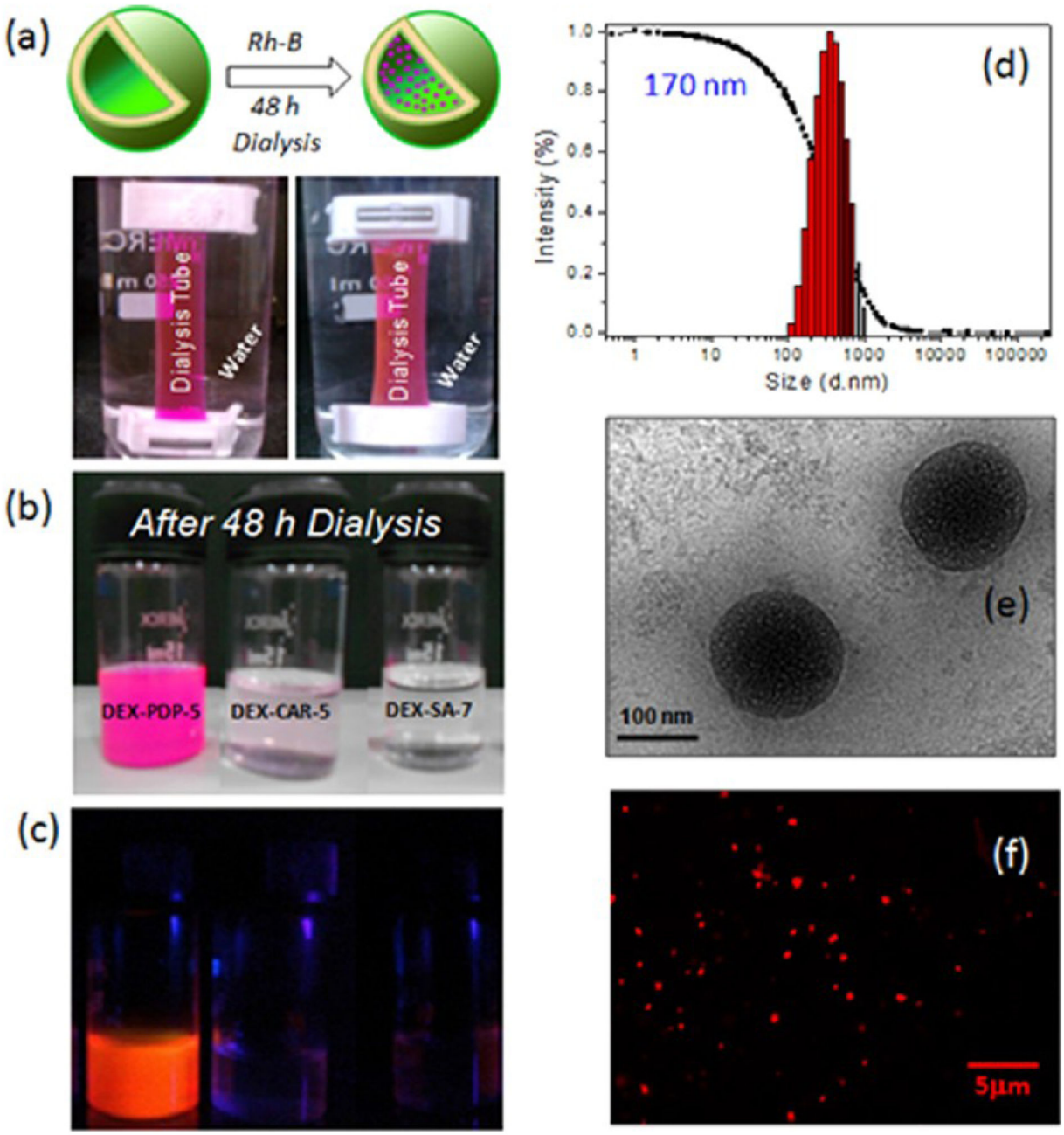

Figure 4.

Schematic representation of the encapsulation of Rhodamine-B in the vesicle and their presence in the dialysis tube (a). Photographs of vials containing the dextran derivatives with Rh-B after 48 h of dialysis (b) and their solution color under photoexcitation (c). DLS histograms (d) and HR-TEM (e) of Rh-B loaded DEX-PDP-5 in PBS (6.2×10^{-5} M). Confocal microscopic image of Rh-B loaded vesicles (f) in PBS (6.2×10^{-3} M).

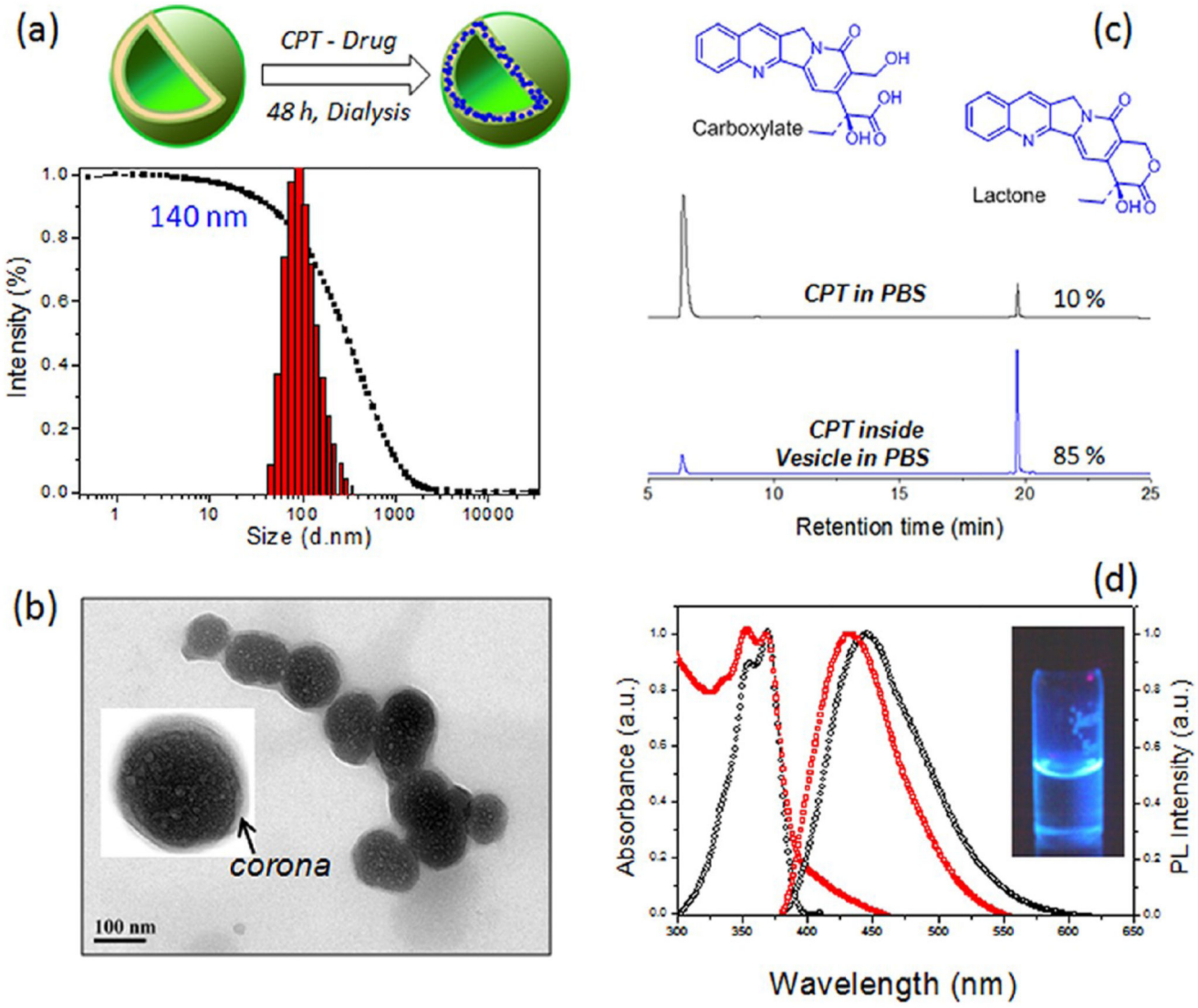

Figure 5.

Schematic representation of the encapsulation of camptothecin in the vesicle and its DLS histograms (a). HR-TEM image of the CPT loaded vesicles (b). The inset showed the expanded image of the vesicles with well-defined corona with respect to vesicular assemblies. HPLC traces of CPT in PBS and encapsulated in the vesicle in the carboxylic and lactone forms (c). Absorbance and fluorescence spectra of CPT loaded vesicles in PBS (d).

Europe PMC Funders Author Manuscripts

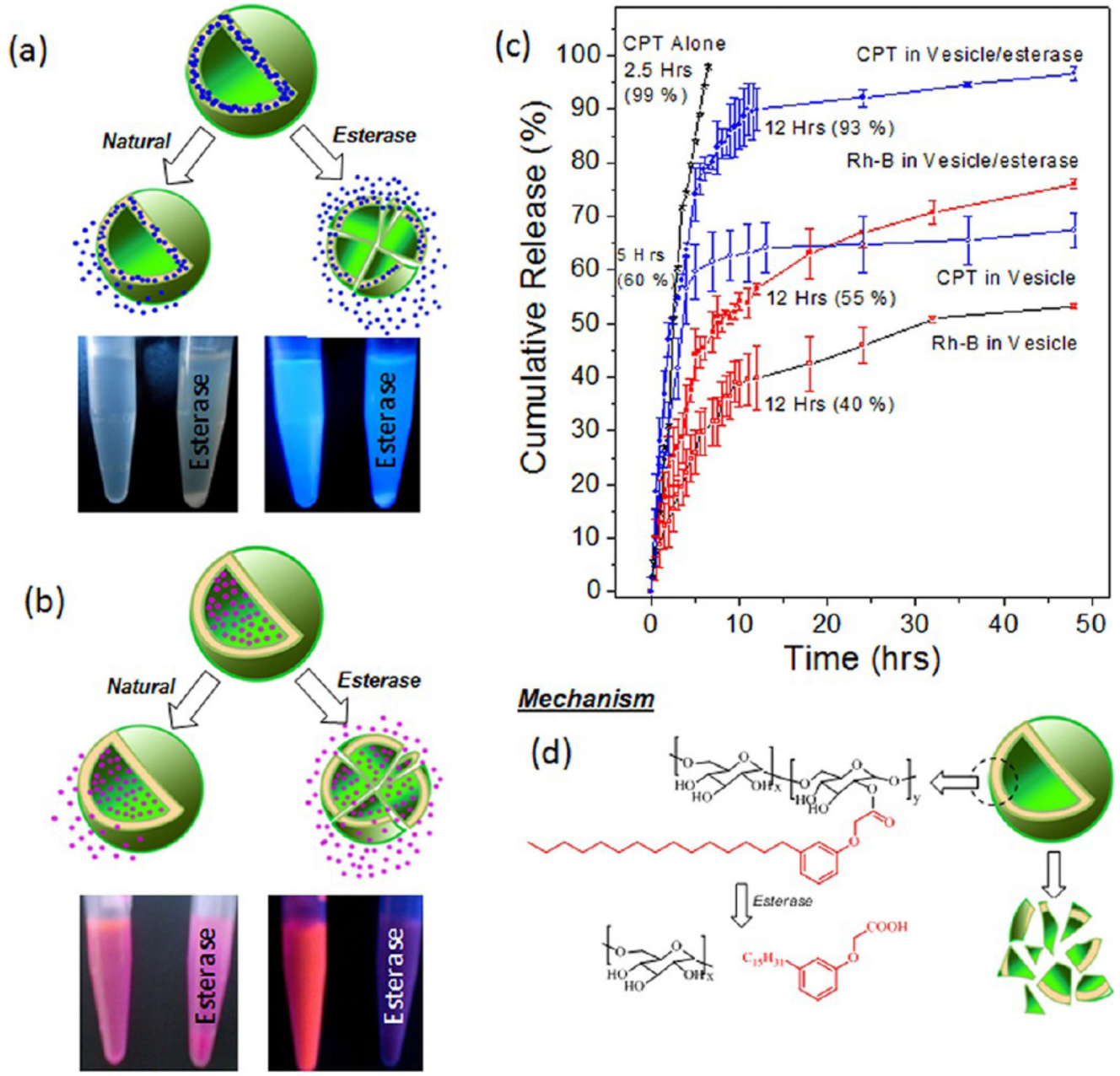

Figure 6.

Schematic drug release of vesicular scaffolds under normal dialysis and in the presence of esterase enzymes. The photographs of the vials showed the formation of precipitate over a prolonged storage of the CPT loaded (a) and Rh-B loaded vesicles (b) in the presence of esterase. The left and right of the vials are corresponding to the Rh-B or CPT loaded vesicles in the absence or presence of esterase, respectively. Cumulative drug release of CPT, CPT loaded vesicles, and Rh-B loaded vesicles (c). The schematic model represents the disassociation of vesicular scaffolds in the presence of esterase (d).

Europe PMC Funders Author Manuscripts

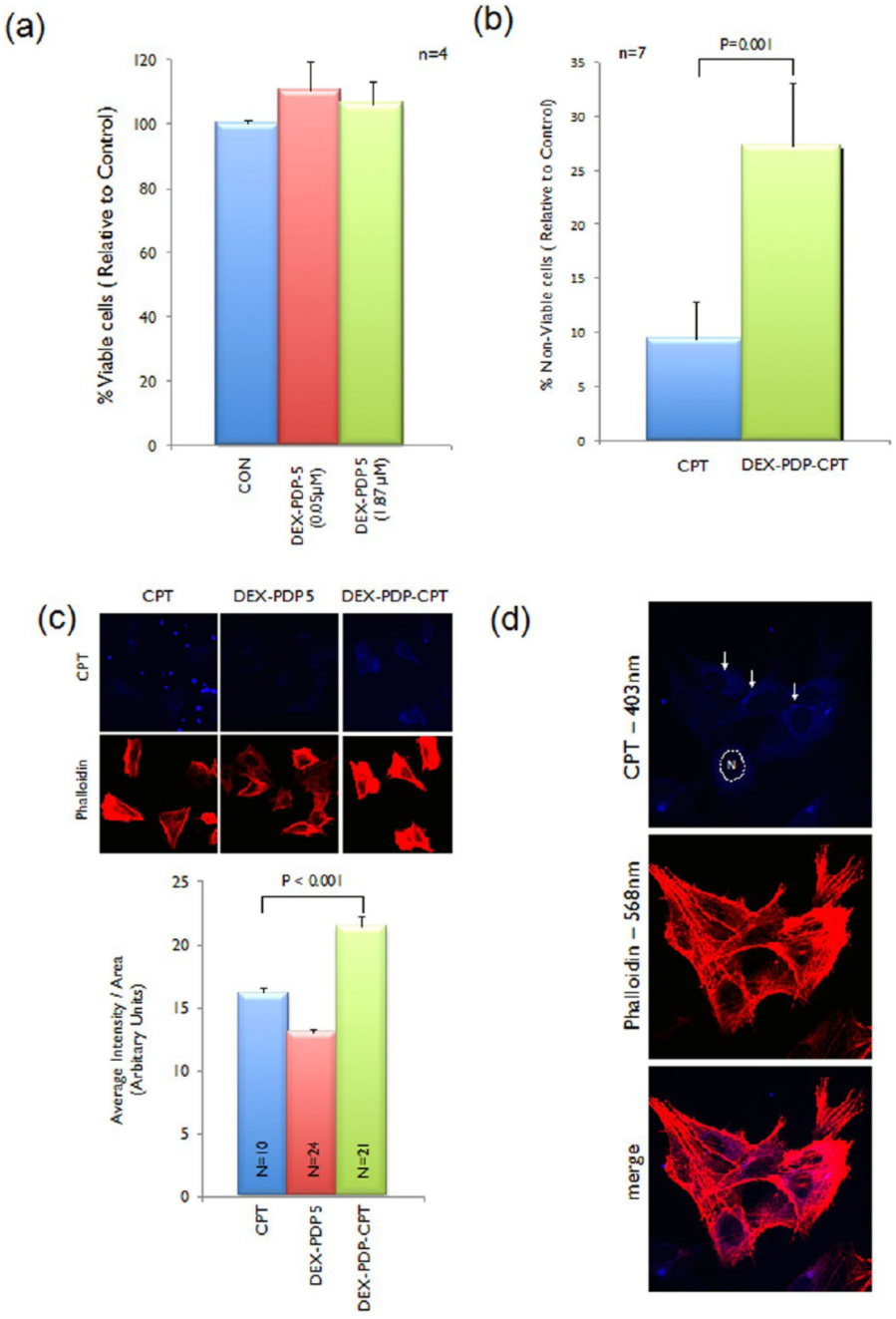

Figure 7.

Cytotoxicity data of DEX-PDP-5 at various concentrations (a) in MTT assay. Cytotoxicity data of CPT and CPT loaded DEX-PDP-5 vesicles in MTT assay (b). Confocal image and quantitation of CPT, DEX-PDP-5, and DEX-PDP-CPT vesicles uptake in cells (c). Localization of CPT loaded DEX-PDP-5 vesicles in cells (d).

Europe PMC Funders Author Manuscripts

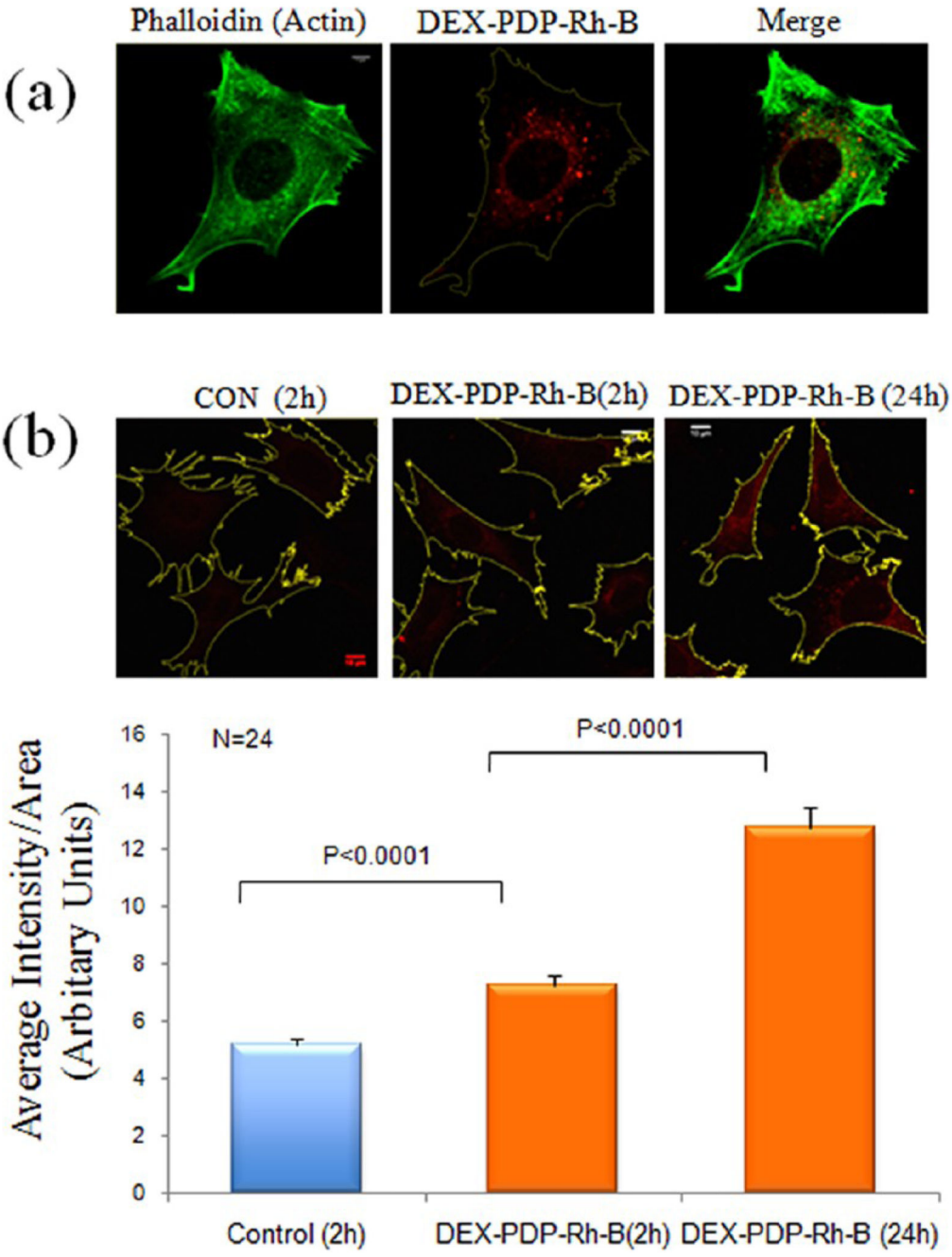

Figure 8.

Endocytosis of DEX-PDP-Rh-B in mouse fibroblasts. (a) Endocytosed DEX-PDP-Rh-B shows a distinct perinuclear localization in mouse fibroblasts. Actin cytoskeletal network in cells is stained with phalloidin. (b) Fluorescence confocal images of control untreated cells and cells incubated with DEX-PDP-Rh-B for 2 and 24 h were recordered, their spread area mapped, and fluorescence intensity in the cell area analyzed using the Image J densitometric software. Mean of fluorescence intensities is represented in the graph.

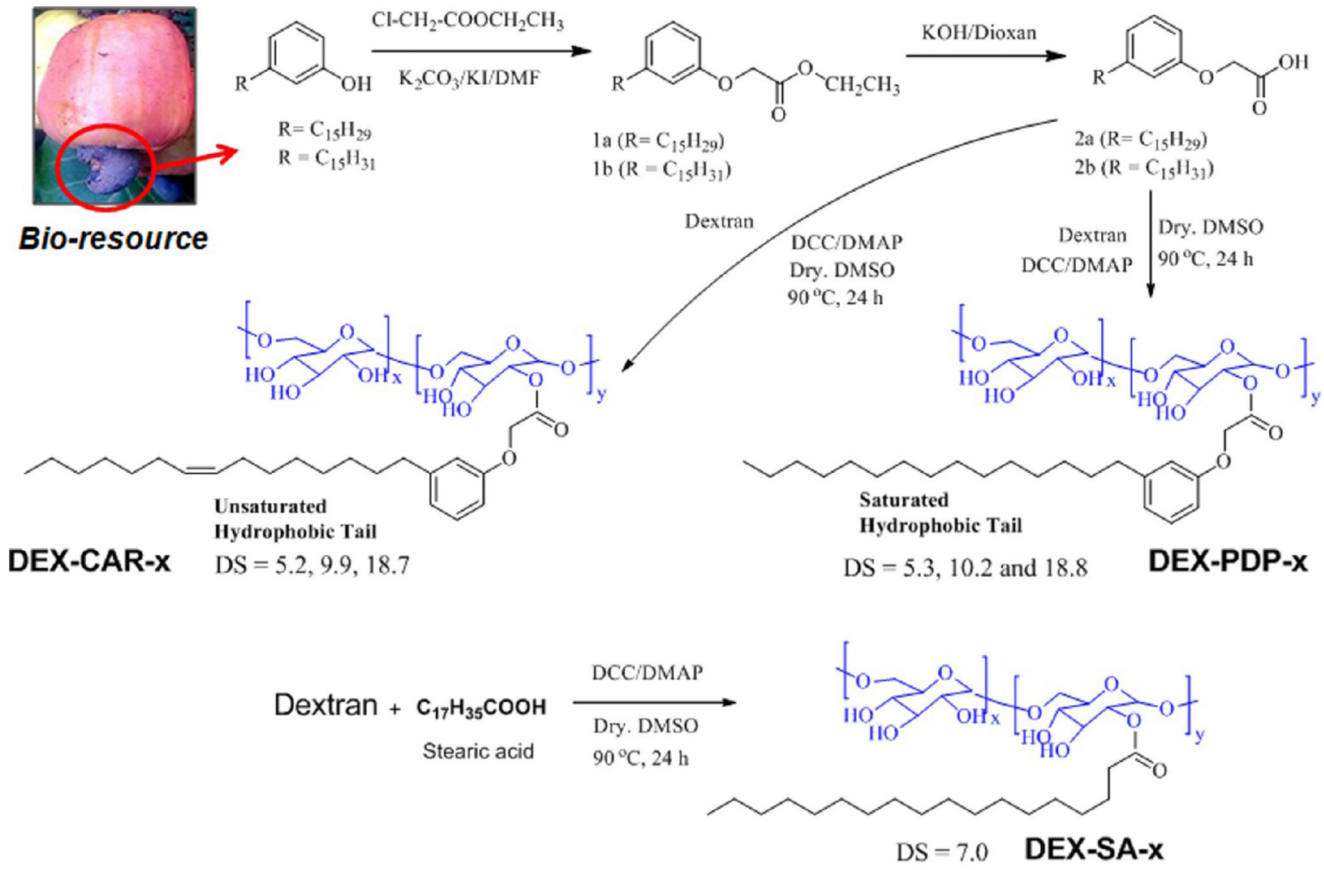

Scheme 1. Synthesis of Dextran Derivatives

Europe PMC Funders Author Manuscripts